

ROBUST OPTICAL RICHNESS ESTIMATION WITH REDUCED SCATTER

E. S. RYKOFF¹, B. P. KOESTER^{2,3}, E. ROZO^{2,3,4}, J. ANNIS⁵, A. E. EVRARD^{6,7,8}, S. M. HANSEN^{9,10}, J. HAO⁵,
D. E. JOHNSTON⁵, T. A. MCKAY^{6,7}, R. H. WECHSLER¹¹

Draft version October 24, 2018

ABSTRACT

Reducing the scatter between cluster mass and optical richness is a key goal for cluster cosmology from photometric catalogs. We consider various modifications to the red-sequence matched filter richness estimator of Rozo et al. (2009b), and evaluate their impact on the scatter in X-ray luminosity at fixed richness. Most significantly, we find that deeper luminosity cuts can reduce the recovered scatter, finding that $\sigma_{\ln L_X|\lambda} = 0.63 \pm 0.02$ for clusters with $M_{500c} \gtrsim 1.6 \times 10^{14} h_{70}^{-1} M_{\odot}$. The corresponding scatter in mass at fixed richness is $\sigma_{\ln M|\lambda} \approx 0.2 - 0.3$ depending on the richness, comparable to that for total X-ray luminosity. We find that including blue galaxies in the richness estimate increases the scatter, as does weighting galaxies by their optical luminosity. We further demonstrate that our richness estimator is very robust. Specifically, the filter employed when estimating richness can be calibrated directly from the data, without requiring a-priori calibrations of the red-sequence. We also demonstrate that the recovered richness is robust to up to 50% uncertainties in the galaxy background, as well as to the choice of photometric filter employed, so long as the filters span the 4000 Å break of red-sequence galaxies. Consequently, our richness estimator can be used to compare richness estimates of different clusters, even if they do not share the same photometric data. Appendix A includes “easy-bake” instructions for implementing our optimal richness estimator, and we are releasing an implementation of the code that works with SDSS data, as well as an augmented maxBCG catalog with the λ richness measured for each cluster.

Subject headings: galaxies: clusters – X-rays: galaxies: clusters

1. INTRODUCTION

In the next few years, a host of large scale optical surveys — e.g. the Dark Energy Survey (DES¹²), the Panoramic Survey Telescope & Rapid Response Systems (Pan-STARRS¹³), Hyper-Suprime Camera (HSC; Takada 2010), and the Large Synoptic Survey Telescope (LSST¹⁴) — are expected to generate galaxy catalogs spanning several thousands of square degrees to sufficient depth to reliably detect galaxies at redshifts as high as $z \approx 1$. These surveys will be used to optically select galaxy clusters, and in conjunction with stacked weak-lensing mass calibration, can be used to place tight

constraints on cosmological parameters (e.g. Rozo et al. 2010a,b; Oguri & Takada 2011).

One of the difficulties confronting cosmology with optical clusters is the fact that optical richness estimates are expected to be noisy tracers of the underlying halo mass.¹⁵ This is particularly problematic because the sensitivity of cluster abundance studies is sensitive to the *uncertainty* in the scatter of the mass–observable relation, and this sensitivity increases with increasing scatter (Lima & Hu 2005). In addition, high scatter increases the sensitivity of cluster abundance measurements to non-Gaussian fluctuations in the observable–mass relation (Shaw et al. 2010), which are often degenerate with cosmological parameters. Consequently, in order to minimize the dilution of the cosmological information of optically selected cluster samples, a richness estimator that minimizes the scatter in the richness–mass relation is highly desirable.

As an example of the magnitude of this problem, we consider the scatter in mass at fixed richness for the maxBCG cluster catalog (Koester et al. 2007a), which is currently the best-studied optically selected cluster catalog at moderate redshifts (e.g. Becker et al. 2007; Rozo et al. 2007; Sheldon et al. 2009a; Johnston et al. 2007; Rykoff et al. 2008; Hansen et al. 2009). Rozo et al. (2009a) finds that the scatter in mass at fixed richness (N_{200}) for maxBCG clusters is $\sigma_{\ln M|N} = 0.45 \pm 0.1$ for clusters with $M_{200} \gtrsim 10^{14} h^{-1} M_{\odot}$. For comparison, X-ray luminosity, which is the noisiest X-ray mass

¹ E. O. Lawrence Berkeley National Lab, 1 Cyclotron Rd., Berkeley CA, 94720, USA

² Department of Astronomy and Astrophysics, The University of Chicago, Chicago, IL 60637, USA

³ Kavli Institute for Cosmological Physics, The University of Chicago, Chicago, IL 60637, USA

⁴ Einstein Fellow

⁵ Center for Particle Astrophysics, Fermi National Accelerator Laboratory, Batavia, IL 60510, USA

⁶ Physics Department, University of Michigan, Ann Arbor, MI 48109, USA

⁷ Astronomy Department, University of Michigan, Ann Arbor, MI 48109, USA

⁸ Michigan Center for Theoretical Physics, Ann Arbor, MI 48109, USA

⁹ UCOLick/Department of Astronomy and Astrophysics, University of California Santa Cruz, Santa Cruz, CA 95064, USA

¹⁰ NSF Astronomy and Astrophysics Postdoctoral Fellow

¹¹ Kavli Institute for Particle Astrophysics and Cosmology; Physics Department, Stanford University; Department of Particle and Particle Astrophysics, SLAC National Accelerator Laboratory; Stanford, CA 94305, USA

¹² <http://www.darkenergysurvey.org>

¹³ <http://pan-starrs.ifa.hawaii.edu>

¹⁴ <http://www.lsst.org>

¹⁵ As discussed in Rozo et al. (2009b), throughout this work the word “richness” is meant to be understood as “optical mass tracer,” and is not necessarily the actual number of cluster galaxies within the virialized region of a cluster or the total optical luminosity of the cluster.

estimator, has a scatter of $\sigma_{\ln M|L_X} = 0.25 - 0.32$ (Vikhlinin et al. 2009; Mantz et al. 2010),¹⁶. This is comparable to the scatter in halo mass at fixed weak lensing mass, which is also estimated to be about $\sigma_{\ln M|WL} = 0.25 - 0.30$ (Becker & Kravtsov 2010). Clearly, there is room for improvement for optical mass tracers.

Indeed, it has been argued on the basis of numerical simulations that the *intrinsic* scatter of the richness–mass relation is Poisson (e.g. Kravtsov et al. 2004; Berlind et al. 2003; Zheng et al. 2005). While recent work indicates the scatter may be significantly super-Poisson at the cluster scale (Boylan-Kolchin et al. 2010; Wetzel & White 2010; Busha et al. 2010), even in this case the intrinsic scatter is expected to be closer to $\sigma_{\ln M|N} = 0.20 - 0.25$ rather than 0.45 at $M_{200} \sim 2 \times 10^{14} M_\odot$, so it is apparent that the maxBCG richness estimator is dominated by extrinsic sources of scatter.

This is the third in a series of papers whose goal is to develop improved richness estimators that are both qualitatively and quantitatively understood in detail. The first of these papers, henceforth referred to as Paper I (Rozo et al. 2009b), laid the fundamental framework of our new optical richness estimator and quantitative techniques. There, we demonstrated that by relying on a *probabilistic* approach toward red sequence color selection, combined with an aperture optimization, one achieves much more robust richness estimates.

In this paper and Paper I (see also Popesso et al. 2004; Lopes et al. 2006) we use X-ray luminosity L_X , as our mass proxy. Our chosen figure-of-merit is the scatter in L_X at fixed richness, $\sigma_{\ln L_X|N}$, where N is an arbitrary richness. The most important reason why we choose this metric is that it is easily available for our large cluster catalog via the ROSAT All-Sky Survey (RASS: Voges et al. 1999). That said, there are strong physical motivations for relying on X-ray luminosities for this study. Specifically, not only is the scatter in mass at fixed L_X smaller than the scatter in mass at fixed richness ($\sigma_{M|L_X} \approx 0.25$ compared to $\sigma_{M|N_{200}} \approx 0.45$), the correlation coefficient between L_X and mass at fixed richness is very nearly unity ($r > 0.9$; Rozo et al. 2009a). That is, at fixed N_{200} , clusters that are brighter in X-rays are also more massive. Consequently, we feel confident that reducing the scatter in the L_X –richness relation will also reduce the scatter in the mass–richness relation. Our final richness estimator from Paper I was easily superior to that of the maxBCG cluster catalog, with a scatter in L_X at fixed richness of $\sigma_{\ln L_X|N} = 0.69 \pm 0.02$, compared to $\sigma_{\ln L_X|N} = 0.86 \pm 0.02$ for the maxBCG richness estimator.

In Rozo et al. (2011, henceforth Paper II), we investigated how extrinsic sources of scatter can impact the observed scatter in the richness–mass relation. In that work, we demonstrated that while optical richness is in principle subject to many sources of noise, in practice only a very small subset of these is observationally relevant. For instance, both photometric errors in galaxy magnitudes/colors and photometric redshift uncertain-

ties in cluster redshifts are unimportant with SDSS-quality data or better. In Paper II we demonstrate that there are two dominant sources of noise. The first, which is an issue for all photometric cluster catalogs, is the density of background galaxies within which a cluster is embedded. Because of galaxy clustering, this background exhibits large cluster-to-cluster fluctuations, so a small percentage of galaxy clusters end up embedded in very large galaxy overdensities. Such occurrences inevitably result in gross richness over-estimates, i.e. projections onto correlated structures. The second is failing to identify the correct center of the galaxy clusters. This effect leads to significant underestimation of cluster richness if the centering offset is comparable to the aperture used to estimate richness, and can be mitigated with improved optical centering algorithms.

In this work, which we refer to as Paper III, we investigate which parameters from Paper I may be changed to further improve the fidelity of our optical richness estimator. By monitoring the change in scatter, $\sigma_{\ln L_X|N}$, we can directly quantify which parameters significantly improve the richness estimator. The specific modifications we consider are whether cluster richness can be improved by counting blue cluster galaxies in addition to the red-sequence galaxies; by summing red-sequence optical luminosity rather than galaxy counts; and the impact of measuring galaxies further down the luminosity function.

In addition to exploring these various modifications, we also test the robustness of our richness estimator to various perturbations, similar to the tests made on simulated data in Paper II. This includes a measurement of the bias and scatter of the richness when different optical filters are used to isolate the red sequence. Finally, we demonstrate the origin of the optimal radial and luminosity cuts using the methods of Paper II.

The end result of this investigation is a new richness estimator that is both robust and, we believe, very close to optimal. Importantly, because this is a stand-alone richness estimator, our method can be applied to any cluster catalog, and can therefore improve optically selected cluster catalogs regardless of how the initial cluster selection is done. Moreover, the insights that we have gained while performing this work are now informing a new cluster finding algorithm that revolves around the probabilistic framework of our richness estimator. A detailed comparison of our richness estimator to other estimators from the literature will be presented in a future paper.

The paper is set up as follows: in Section 2 we introduce the data sets upon which our analysis is based. Section 3 briefly reviews the richness estimator from Paper I and sets up the probabilistic framework employed in this paper. Section 4 describes how we define our figure-of-merit for assessing improvement in optical richness estimation, as well as the various modifications we consider. Section 5 tests the robustness of our richness estimator to various sources of systematic errors, most notably the choice of filters used to select red-sequence galaxies, as well as the exact values of the model parameters that define the filter employed in our richness estimates. Section 6 follows the work of Paper II to show the origin of the optimal radial and luminosity cuts. Our conclusions are presented in Section 7. We have also summarized

¹⁶ Vikhlinin et al. (2009) quote $\sigma_{\ln L_X|M} = 0.396$, and $L_X \propto M^{1.61}$, which corresponds to a scatter in mass at fixed L_X of $\sigma_{\ln M|L_X} = 0.396/1.61 = 0.25$. The same calculation using the results of Mantz et al. (2010) gives $\sigma_{\ln M|L_X} = 0.32$.

all the relevant information required to code our new richness estimator in Appendix A. Finally, Appendix B provides a tentative mass–richness relation for our optimal estimator. We emphasize, however, that the problem of deriving a robust calibration, with well characterized uncertainties, is left for future work.

2. DATA

All data used in this work comes from two large area surveys, the Sloan Digital Sky Survey (SDSS; York et al. 2000) and the ROSAT All-Sky Survey (RASS; Voges et al. 1999). SDSS imaging data is used to select clusters and to measure their matched filter richness, while RASS data provides 0.1–2.4 keV X-ray fluxes for each cluster.

The input data and analysis in this work is similar to Paper I, although there are some key differences noted below. Of particular note is the change from an input galaxy catalog based on SDSS DR4 to one based on SDSS DR7. Here we summarize the key aspects of the analysis. For full details see Paper I.

2.1. Cluster Sample

Following Paper I, cluster locations, redshift estimates, and initial richness estimates are taken from the maxBCG cluster catalog (Koester et al. 2007a,b), an optically selected cluster catalog. The maxBCG algorithm identifies galaxy clusters by relying on the observation that the galaxy population of massive halos clusters tightly in space and color, forming what is known as the E/S0 ridgeline or red-sequence (e.g. Dressler 1984; Kormendy & Djorgovski 1989; Hansen et al. 2009). This feature allows for high-contrast detection of galaxy clusters with optical data, both locally and out to high redshift (e.g. Gladders & Yee 2000; Eisenhardt et al. 2008).

The maxBCG catalog is approximately volume limited in the redshift range of interest ($0.1 \leq z \leq 0.3$), with very accurate cluster photometric redshifts ($\delta z \sim 0.01$). Studies with mock SDSS catalogs indicate that the completeness and purity are above 90% (Koester et al. 2007a; Rozo et al. 2007). The maxBCG catalog has been used to investigate the scaling of multiple cluster mass proxies with richness, including line-of-sight velocity dispersion (Becker et al. 2007), X-ray luminosity (Rykoff et al. 2008), and weak lensing shear (Sheldon et al. 2009a), as well as derive cosmological constraints from cluster counts (Roza et al. 2007, 2010a).

The richness estimator used in the maxBCG catalog is N_{200} , defined as the number of galaxies with $g - r$ colors within 2σ of the E/S0 ridgeline as defined by the BCG color, that are brighter than $0.4 L_*$ (in i -band), and found within a scaled aperture r_{200}^{gal} of the cluster center (Hansen et al. 2005). The full catalog comprises 13,823 objects with a richness threshold $N_{200} \geq 10$, corresponding to $M \gtrsim 5 \cdot 10^{13} h^{-1} M_{\odot}$ (Johnston et al. 2007).

2.2. X-ray Measurements

The scatter in L_X at fixed richness, $\sigma_{\ln L_X|N}$ (where N is an arbitrary richness) is estimated using the methods of Paper I and Rykoff et al. (2008). In brief, we use the RASS photon maps to estimate the 0.5–2.0 keV X-ray flux at the location of each cluster, which is turn

used to derive L_X [0.1–2.4 keV] given the cluster’s photometric redshift (the conversion factors are similar to those used in Böhringer et al. 2004). We then perform a Bayesian linear regression to $\ln L_X$ as a function of $\ln N$, where N is the richness parameter to be tested. The variance in $\ln L_X$ is included as a free parameter. The fit is done following the algorithm presented in Kelly (2007), and correctly takes into account errors on the independent variable as well as upper limits on L_X for those clusters without significant detection of X-ray emission. This method has several advantages, in that it takes into account all the available X-ray data, not only that for clusters in X-ray catalogs.

When estimating L_X , one must specify an aperture. The matched filter richness estimators described in this paper have the benefit of assigning a cluster radius R_c , to each individual cluster. As in Paper I, we estimate L_X using the aperture derived from the cluster richness. Alternatively, using a fixed $0.9 h^{-1}$ Mpc aperture to estimate L_X does not have a significant effect on our results.

As discussed in Rykoff et al. (2008, see Section 5.6), there is clear evidence that strong cool core clusters increase the scatter in X-ray cluster properties. High resolution X-ray imaging of clusters allows the exclusion of cluster cores, reducing the scatter in observed X-ray properties (e.g. O’Hara et al. 2006; Chen et al. 2007; Maughan 2007). Unfortunately, the broad PSF of *ROSAT* means that it is impossible to do so in this work. In Paper I, we analyzed both the full sample of maxBCG clusters as well as a “clean” sample after removing all 10 known strong cool core maxBCG clusters that may significantly bias our results (see Section 2.4 in Paper I). We concluded that although the absolute value of the scatter in L_X at fixed richness is reduced by using the “clean” sample, the same general trends were evident with the full and “clean” samples. In this work, we focus exclusively on the “clean” sample of Paper I.

2.3. Input Galaxy Catalog

The input galaxy catalog for this work is derived from SDSS DR7 data (Abazajian et al. 2009). This data release includes nearly 10000 square degrees of drift-scan imaging in the Northern Galactic Cap. However, as the maxBCG cluster catalog was created using data from DR4 (Adelman-McCarthy et al. 2006), the relevant area covered is ~ 7500 square degrees. Survey edges, regions of poor seeing, and bright stars are masked as previously described (Scranton et al. 2002; Koester et al. 2007a; Sheldon et al. 2009b). In this work we use `CMODEL_COUNTS` as our total magnitude, and `MODEL_COUNTS` when computing colors. All magnitudes are corrected for Galactic extinction.

The careful selection of a clean input catalog is required for proper richness estimation. In Section 5.6 we discuss the effects of “catalog noise” on the richness–mass relation, by which we mean the inclusion of stars and/or artifacts as well as catastrophic photometric errors in the galaxy catalog employed when estimating richnesses. Our best input catalog was based on the same cuts used in Sheldon et al. (2009b). After selecting galaxies based on the default SDSS star/galaxy separator, we filter all objects with any of the following flags set in the $g, r,$ or i bands: `SATURATED`, `SATUR_CENTER`, `BRIGHT`, `NOPESTRO`, `DEBLENDED_AS_MOVING`. These cuts remove \sim

30% of the objects brighter than $i > 22$, including a significant number of relatively bright stars that are erroneously tagged as galaxies in the SDSS pipeline.

3. THE MATCHED FILTER RICHNESS λ

Working within the same theoretical framework as Paper I, we now attempt to improve upon the richness estimator λ advocated in that paper. Consequently, we now review the richness estimator λ as described in Paper I.

Let \mathbf{x} be a vector describing the observable properties of a galaxy (e.g. galaxy color, magnitude, and position). We model the projected galaxy distribution around clusters as a sum $S(\mathbf{x}) = \lambda u(\mathbf{x}|\lambda) + b(\mathbf{x})$ where λ is the number of cluster galaxies, $u(\mathbf{x}|\lambda)$ is the cluster's galaxy density profile normalized to unity, and $b(\mathbf{x})$ is density of background (i.e. non-member) galaxies. The probability that a galaxy found near a cluster is actually a cluster member is simply

$$p(\mathbf{x}) = \frac{\lambda u(\mathbf{x}|\lambda)}{\lambda u(\mathbf{x}|\lambda) + b(\mathbf{x})}. \quad (1)$$

The total number of cluster galaxies λ must satisfy the constraint equation

$$\lambda = \sum p(\mathbf{x}|\lambda) = \sum_{R < R_c(\lambda)} \frac{\lambda u(\mathbf{x}|\lambda)}{\lambda u(\mathbf{x}|\lambda) + b(\mathbf{x})}. \quad (2)$$

The corresponding statistical uncertainty in λ is given by (see Paper II)

$$\text{Var}(\lambda) = \sum p(\mathbf{x}|\lambda) [1 - p(\mathbf{x}|\lambda)]. \quad (3)$$

In principle, these sums should extend over all galaxies. In practice, one needs to add over all galaxies within some cutoff radius R_c and above some luminosity cut L_{cut} . In Paper I, L_{cut} was set to $L_{cut} = 0.4L_*$, while the radial cut was assume to scale as a power-law with λ , such that

$$R_c(\lambda) = R_0(\lambda/100.0)^\beta. \quad (4)$$

The most important thing to note about Eqns. 2 and 4 is that *the cluster richness is the only unknown*. Consequently, one can numerically solve Eqn. 2 for λ using simple zero-finding algorithm. This automatically produces a cluster radius estimate R_c via equation 4.

In Paper I we considered three observable properties of galaxies: R , the projected distance from the cluster center; m , the galaxy i -band magnitude; and c , the galaxy $g - r$ color. We adopted a separable filter function

$$u(\mathbf{x}) = [2\pi R \Sigma(R)] \phi(m) G(c), \quad (5)$$

where $\Sigma(R)$ is the two dimensional cluster galaxy density profile, $\phi(m)$ is the cluster luminosity function (expressed in apparent magnitudes), and $G(c)$ is color distribution of cluster galaxies. The prefactor $2\pi R$ in front of $\Sigma(R)$ accounts for the fact that given $\Sigma(R)$, the radial probability density distribution is given by $2\pi R \Sigma(R)$. In Paper I, we showed that the color filter is by far the most important of the three filters in reducing the scatter. We summarize below the specific filters employed in Paper I.

3.1. The Radial Filter

For the radial filter, Paper I adopted an NFW profile (Navarro et al. 1995), which is a good description of the dark matter profile in N-body simulations,

and is found to be a good descriptor of the distribution of cluster galaxies (Lin & Mohr 2004; Hansen et al. 2005; Popesso et al. 2007). The corresponding two-dimensional surface density profile is (Bartelmann 1996)

$$\Sigma(R) \propto \frac{1}{(R/R_s)^2 - 1} f(R/R_s), \quad (6)$$

where R_s is the characteristic scale radius, and

$$f(x) = 1 - \frac{2}{\sqrt{x^2 - 1}} \tan^{-1} \sqrt{\frac{x-1}{x+1}}. \quad (7)$$

This formula assumes $x > 1$. For $x < 1$, one uses the identity $\tan^{-1}(ix) = i \tanh(x)$.

Following Koester et al. (2007a), Paper I set $R_s = 0.15 h^{-1} \text{Mpc}$. Also, in order to avoid the singularity at $R = 0$, they assumed Σ was constant for $R \leq R_{core} = 0.1 h^{-1} \text{Mpc}$. This core density is chosen so that the mass distribution $\Sigma(R)$ is continuous. Finally, the profile $\Sigma(R)$ is truncated at the cluster radius $R_c(\lambda)$, and is normalized such that

$$1 = c \int_0^{R_c(\lambda)} dR 2\pi R \Sigma(R). \quad (8)$$

For the NFW profile with the given values of R_s and R_c , the normalization factor c can be parametrized as

$$c = \exp(1.6517 - 0.5479\rho + 0.1382\rho^2 - 0.0719\rho^3 - 0.01582\rho^4 - 0.00085499\rho^5), \quad (9)$$

where $\rho = \ln(R_c)$ and $0.001 < R_c < 3$.

3.2. The Luminosity Filter

The luminosity distribution of maxBCG clusters is well represented by a Schechter function (e.g. Hansen et al. 2009) which we write as

$$\phi(m) \propto 10^{-0.4(m-m_*)(\alpha+1)} \exp\left(-10^{-0.4(m-m_*)}\right). \quad (10)$$

Paper I set $\alpha = 0.8$ independent of redshift. The characteristic magnitude, m_* , is calculated for a k -corrected passively evolving stellar population (Koester et al. 2007b). We assume $M_*^i = -21.22$ for red galaxies, corresponding to $2.25 \times 10^{10} L_\odot$. A PEGASE.2 stellar population/galaxy formation model (e.g. Eisenstein et al. 2001) was used to calculate the k -corrected magnitude at each redshift. In the redshift range $0.05 < z < 0.35$ appropriate for maxBCG, $m_*(z)$ is well approximated by a fourth order polynomial:

$$m_*(z) = 12.27 + 62.36z - 289.79z^2 + 729.69z^3 - 709.42z^4. \quad (11)$$

For each cluster, m_* is taken at the appropriate redshift and the filter is normalized by integrating down to the magnitude cutoff. In Paper I, this was chosen to be $0.4L_*$, or $m_* + 1 \text{ mag}$.

3.3. The Color Filter

The old stellar populations in the red sequence galaxies have a prominent 4000 \AA break in their spectra. In the redshift range targeted by maxBCG, $z \lesssim 0.35$, the 4000 \AA break is located in the g band. Therefore, the $g - r$ color of red-sequence galaxies correlates strongly with redshift, and results in tight E/S0 ridgelines. Consequently, Paper I relied on $c = g - r$ for their color

filter. They assume $G(c)$ is Gaussian with a small intrinsic dispersion of $\sigma_{\text{int}} = 0.05$ mag. The corresponding color filter, $G(c)$ is

$$G(c|z) = \frac{1}{\sqrt{2\pi}\sigma} \exp\left[-\frac{(c - \langle c|z \rangle)^2}{2\sigma^2}\right], \quad (12)$$

where $c = g - r$ is the color of interest, $\langle c|z \rangle$ is the mean of the Gaussian color distribution of early type galaxies at redshift z , and the net dispersion σ is the sum in quadrature of the intrinsic color dispersion $\sigma_{\text{int}} = 0.05$ and the estimated color error σ_c . The mean color $\langle c|z \rangle = 0.625 + 3.149z$ was determined by matching maxBCG cluster members to the SDSS LRG (Eisenstein et al. 2001) and MAIN (Strauss et al. 2002) spectroscopic galaxy samples. In Section 4.3 we investigate modifications of this color model based on measurements of the red sequence of maxBCG clusters measured in Hao et al. (2009).

3.4. Background Estimation

The last necessary ingredient for estimating λ is a background model. We assume the background galaxy density is constant in space, so that $b(\mathbf{x}) = 2\pi R \bar{\Sigma}_g(m_i, c)$ where $\bar{\Sigma}_g(m_i, c)$ is the galaxy density as a function of galaxy i -band magnitude and $g - r$ color. The mean galaxy density is obtained by binning the full galaxy catalog in color and magnitude using a cloud-in-cells (CIC) algorithm (e.g. Hockney & Eastwood 1981) and dividing by the survey area. For our cells, we use 40 evenly-spaced bins in $g - r \in [-1, 3]$ and 100 bins in $i \in [12, 22]$. The final galaxy number density is normalized by the width of each color and magnitude bin (0.1 mags each). We mark as “bad” all cells that have fewer than 5 galaxies/sq. deg. This has the effect of masking out erroneous photometric artifacts that are called bright galaxies in the DR7 catalog. Although these artifacts are rare, they may nevertheless significantly bias the luminosity-weighted richness for a few clusters (see Section 4.6).¹⁷ We emphasize that because the background is measured per square degree, the average number of background galaxies is automatically accounted for as the angular size of the clusters changes with redshift.

4. IMPROVING λ

We now explore whether we can further improve upon the results of Paper I in a variety of ways. We define our metric to assess improvement in a richness estimator in Section 4.1. Section 4.2 tests the impact of modifying the color filter to account for the blue galaxy population of cluster galaxies. In Section 4.3 we take into account the small but non-zero tilt in the ridgeline. Section 4.4 explores the effect of the luminosity cut on the L_X -richness relation, and Section 4.5 focuses on the importance of the choice of the radial filter function. Finally, in Section 4.6 we investigate whether red sequence luminosity is a better L_X tracer than λ . Throughout this discussion, we have adopted a fixed metric aperture $R_c = 0.9 h^{-1}$ Mpc for estimating richness, which we demonstrated in Paper I was near optimal for the cluster sample under consideration. In section 4.7 we relax this assumption and optimize our choice of aperture.

¹⁷ We note that Paper I relied on random point sampling to estimate $\bar{\Sigma}_g$ rather than making use of the full survey area. This does not impact our results in any way.

4.1. Richness Testing Methodology: What Constitutes an Improved Richness Estimate?

The primary goal of this paper is to improve upon the Paper I richness estimator. To do that, however, we must first define the metric used to gauge improvement. As discussed in the Introduction, our chosen figure-of-merit is the scatter in L_X at fixed richness. As in Paper I, we limit ourselves to the richest 2000 clusters as ranked by the richness estimate under consideration so that our results are insensitive to the $N_{200} \geq 10$ cut in the maxBCG catalog. For the original maxBCG richness estimator N_{200} , this is equivalent to $N_{200} \geq 20$, or an equivalent mass of $M_{200} \gtrsim 1 \times 10^{14} h^{-1}$ Mpc (Johnston et al. 2007). In Paper I we confirmed that our results with the top 1000 or 3000 clusters are consistent with the top 2000.

We denote the original matched filter richness estimator described in Paper I as λ_0 . Using the top 2000 richest clusters in the clean sample, and a fixed $0.9 h^{-1}$ Mpc aperture, we find $\sigma_{\ln L_X|\lambda_0} = 0.69 \pm 0.02$.¹⁸ As discussed in Section 5.3 of Paper I, comparing two richnesses is complicated by the fact that the errors are correlated. In all pairwise richness comparisons, we perform bootstrap resampling on the clean cluster catalog and calculate the scatter in the top 2000 clusters for both λ_0 and the new richness λ_{new} . For each bootstrap resampling we calculate $r = \sigma_{\ln L_X|\lambda_{\text{new}}} / \sigma_{\ln L_X|\lambda_0}$. If the improvement in scatter is not significant, we will find that r is consistent with unity, whereas an improved (worse) scatter will result in an r value that is significantly less than (greater than) 1. This is our primary diagnostic for improvement.

In addition to the scatter, we also monitor the redshift evolution in the L_X -richness relation of each of the richness estimators we consider to ensure that no strong redshift evolution is introduced by our alterations. We measure the evolution using a stacking analysis as described in Paper I and Rykoff et al. (2008, see Section 5.3). In brief, we measure $\langle L_X|N \rangle$ where N is the richness measure of interest in three different redshift bins ($0.10 < z < 0.18$; $0.18 < z < 0.26$; and $0.26 < z < 0.30$). As shown in Rykoff et al. (2008), the stacking analysis allows us to go much further down the richness function than for the scatter analysis. While this introduces selection function effects near the $N_{200} \geq 10$ threshold of the maxBCG cluster catalog, we expect these to be minor in the redshift evolution, which, as mentioned earlier, we only use as a sanity check. We fit the stacked data with a power-law evolution in redshift,

$$\langle L_X|N \rangle = A \left(\frac{N}{40}\right)^\alpha \left(\frac{1+z}{1+\tilde{z}}\right)^\gamma, \quad (13)$$

where \tilde{z} is the median redshift of the cluster sample and N is the richness measure of interest. We find that $\gamma = 0.7 \pm 0.8$ for λ_0 , consistent with no evolution.

As noted in Paper I, even if the relation between N and cluster mass is redshift independent, we may expect to observe evolution in the $L_X - N$ relation due to evolution in the $L_X - M$ relation. The expectation for self-similar evolution in L_X at fixed mass is $L_X \propto \bar{\rho}_c$ for soft-band X-ray luminosities (Kaiser 1986), where ρ_c is the critical density of the Universe at redshift z . In a Λ CDM Universe with $\Omega_m = 0.25$, $L_X \propto \rho_c$ is well approximated by

¹⁸ We note that we get consistent values with DR4 and DR7 photometry; see also Section 5.6.

$L_X \propto (1+z)^{1.10}$, or $\gamma = 1.10$. Thus, for λ_0 , the evolution is consistent with both the no-evolution and the self-similar evolution models. As we do not know what the true evolution should be, we do not use the evolution parameter γ as a true comparison between richness estimators. That said, modest evolution in the richness–mass relation is a desirable property for richness estimators, so we do check that γ remains in the range $\approx 0–1.5$ as we modify λ .

4.2. Blue Cluster Members

The red sequence is well-suited to cluster finding due to its high contrast with the background, and its strong redshift dependence (e.g. Bower et al. 1992; Gladders & Yee 2000; Koester et al. 2007a). However, not all cluster galaxies are red, only the majority, with typical red-fractions being of order $\approx 80\%$ (e.g. Hao et al. 2009). We now explore whether accounting for this blue galaxy population in our color filter improves our richness estimator.

We first empirically construct a new color filter that accounts for both red and blue galaxies. As an input, we use the 2000 richest clusters as measured by our original matched filter richness estimator, λ_0 . We then bin these clusters in 10 redshift bins of width 0.02, and select all galaxies within $0.9 h^{-1}$ Mpc of the BCG brighter than $0.4L_*$. To estimate galaxy luminosity, we assume all galaxies are at the cluster redshift. The empirical color distribution of these galaxies is then background subtracted and fit as a sum of two Gaussians using the Error Corrected Gaussian Mixture Model (ECGMM) of Hao et al. (2009), which allows us to properly take into account photometric errors. The location, width, and relative amplitude of these two Gaussians define the appropriate color filter for the color distribution of all (red+blue) cluster galaxies within our chosen aperture. Additional tests have shown that the color distribution does not depend significantly on cluster richness λ_0 .

Figure 1 shows our best fit model (solid green line) for the lowest redshift bin ($0.1 < z < 0.12$) and the highest redshift bin ($0.28 < z < 0.30$). Note our best fit model is narrower than the binned histogram since the latter is broadened by photometric errors, particularly in the case of our high redshift bin.

Our empirically determined model filter takes the form

$$G(c|z) = \frac{\alpha_{\text{red}}}{\sqrt{2\pi}\sigma_{\text{red}}} \exp\left[-\frac{(c - \mu_{\text{red}})^2}{2\sigma_{\text{red}}^2}\right] + \frac{\alpha_{\text{blue}}}{\sqrt{2\pi}\sigma_{\text{blue}}} \exp\left[-\frac{(c - \mu_{\text{blue}})^2}{2\sigma_{\text{blue}}^2}\right], \quad (14)$$

where α_{red} and α_{blue} are the relative weights of the red and blue Gaussians; μ_{red} and μ_{blue} are the mean color of the red and blue galaxies at redshift z ; and $\sigma_{\text{red,int}}$ and $\sigma_{\text{blue,int}}$ are the intrinsic scatter for the red and blue galaxies. Each of these parameters is fit as a function of redshift using a simple linear relation, with the exception of the Gaussian widths, which we find is consistent with no evolution. Our final model parameters are

$$\mu_{\text{red}} = 0.629 + 3.016z \quad (15)$$

$$\mu_{\text{blue}} = 0.590 + 2.115z \quad (16)$$

$$\alpha_{\text{red}} = 0.786 - 0.303z \quad (17)$$

$$\alpha_{\text{blue}} = 1.0 - \alpha_{\text{red}} \quad (18)$$

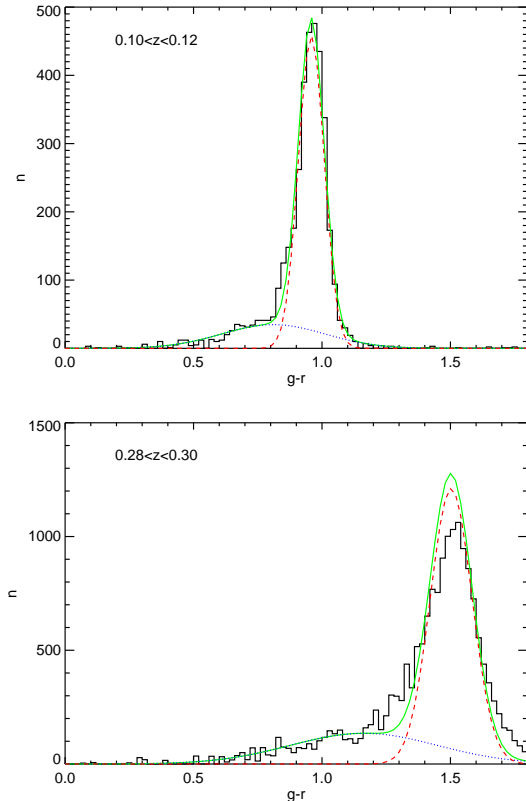


FIG. 1.— Color histograms of maxBCG clusters in the lowest redshift bin (top panel) and the highest redshift bin (bottom panel). The black histogram comprises the total of cluster members brighter than $0.4L_*$ within $0.9 h^{-1}$ Mpc, after subtracting out the predicted number of background galaxies. The green curve is our best fit double-Gaussian model, taking into account the “observational broadening” brought about by photometric errors. This explains why our best fit model is narrower than histogram, particularly for our high redshift bin.

$$\sigma_{\text{red,int}} = 0.05 \quad (19)$$

$$\sigma_{\text{blue,int}} = 0.25. \quad (20)$$

We can now replace the Gaussian color filter in Eqn. 12 with this new filter, and combine it with the original luminosity and radial filters to measure a new richness, $\lambda_{\text{red+blue}}$. The scatter in L_X at fixed richness is $\sigma_{\ln L_X | \lambda_{\text{red+blue}}} = 0.72 \pm 0.02$, and the corresponding redshift evolution parameter is $\gamma = 0.1 \pm 0.6$. We note that the width of the color filter for the blue cluster members derived here is slightly wider than that derived from spectroscopically confirmed subsamples (Hao et al. 2009), implying that there is some contamination from background galaxies. However, further tests have confirmed that our results are insensitive to the precise width of this component (see also Section 5.3).

To measure the significance of the change, we use the bootstrap resampling described in Section 4.1, and find $r = 1.04 \pm 0.02$. That is, including the blue galaxies in the filter *increases* the scatter at a significance of 2σ . This may be due to the fact that measuring blue cluster members is inherently noisier due to the smaller contrast with the background, or it may reflect that blue galaxies in clusters tend to have fallen in more recently (e.g.

Abraham et al. 1996), thereby adding stochasticity to the richness measure. Adequately addressing this issue would require us to repeat this analysis using full spectroscopic membership information, which we do not currently have available for this sample. We also note the possible correlation of the radial and luminosity filters with the color filter, as blue cluster galaxies are generally fainter and further from the core than the red galaxies (e.g., Hansen et al. 2009). However, as we show in Paper I, the color filter is dominant so we do not expect this to be a significant issue. We conclude that attempting to include blue galaxies in richness estimates when only photometric data is available will *increase* the scatter of the L_X –richness relation.

4.3. Red Sequence Tilt

Thus far, we have treated the color of the red sequence cluster members as a function of redshift only. However, in addition to a zero-point (mean color) and scatter, the ridgeline has a slope in color-magnitude space: fainter (less massive) galaxies have bluer colors, possibly reflecting trends from the mass-metallicity relation (e.g. Kodama & Arimoto 1997; Bernardi et al. 2005; De Lucia et al. 2007). In this section, we investigate the effect of red sequence tilt and its redshift evolution on the matched filter richness estimation.

Hao et al. (2009) used the maxBCG cluster catalog to measure the slope and intercept of the $g - r$ vs. i color-magnitude relation for red-sequence galaxies. They find that the ridgeline slope is nearly independent of cluster richness, consistent with findings that the slope is independent of environment (Hogg et al. 2004). The color filter that incorporates this tilt is described as follows:

$$G(c, m|z) = \frac{1}{\sqrt{2\pi}\sigma} \exp\left[-\frac{d(c, m|z)^2}{2\sigma^2}\right], \quad (21)$$

where

$$d(c, i|z) = c - (m_{17}(i - 17.0) + b_{17}). \quad (22)$$

The slope and zero-point at $i = 17$ are taken from Hao et al. (2009):

$$m_{17} = -0.0701z - 0.008969 \quad (23)$$

$$b_{17} = 3.2982z + 0.58907. \quad (24)$$

As before, $c = g - r$ is the relevant color and m denotes the i band magnitude. The net dispersion σ is taken as the sum in quadrature of the intrinsic color dispersion $\sigma_{int} = 0.05$ and the estimated color error σ_c .¹⁹

After replacing the Gaussian color filter in Eqn. 12 with the tilt-based filter in Eqn. 21, we measure the new richness λ_{tilt} . The scatter in L_X for the new richness is $\sigma_{\ln L_X|\lambda_{\text{tilt}}} = 0.69 \pm 0.02$, and the corresponding redshift evolution parameter $\gamma = 1.3 \pm 0.5$. The change in scatter is insignificant, with $r = 0.996 \pm 0.01$. Therefore, incorporating the tilt of the red sequence *does not make a significant difference* in the scatter or redshift evolution.

This is not particularly surprising: not only is the tilt of the red sequence small compared to the intrinsic scatter,

in Paper I we demonstrated that the adopted Gaussian color filter was very robust relative to small systematic offsets between the center of the filter and the true mean color of cluster galaxies. That said, the tilt of the red sequence evolves with redshift, becoming increasingly important at higher redshifts. Thus, it is possible — even likely — that our above conclusion will not hold at high redshifts, or when extending λ to fainter luminosities, thereby increasing the lever-arm over which the tilt of the red sequence can act. Therefore, despite the fact that we do not observe a significant improvement, we have opted to incorporate the tilt-based color filter from Eqn. 12 into our standard definition of λ for further tests.

4.4. Going Deeper

When estimating richness, one must adopt a luminosity or magnitude cut. In Paper I, we adopted a luminosity cut $L_{cut} = 0.4L_*$, which was chosen to allow consistent richness estimates across the entire survey volume ($0.1 \leq z \leq 0.3$) while maintaining high precision photometry for the faintest galaxies considered. However, this cut is not uniquely specified by these conditions. The full DR7 input catalog is complete to $i \approx 21.3$, which corresponds to a luminosity of $0.1L_*$ at a redshift of $z = 0.3$, so we can easily go deeper. We now explore whether doing so can reduce the scatter in the richness–mass relation.

We have calculated the matched filter richness λ for a set of luminosity cuts: $L_{cut}/L_* = \{0.10, 0.15, 0.20, 0.25, 0.30, 0.35, 0.40\}$ for every maxBCG cluster.²⁰ For this test, we use the color filter including the red-sequence tilt, as described in the previous section.

Figure 2 shows the comparison of the scatter in L_X at fixed richness for different luminosity cuts for the top 2000 clusters (black diamonds). We find that there does in fact appear to be an optimal luminosity cut $L_{cut} = 0.2L_*$ ($m_* + 1.75$ mag) below which λ fails to improve any further. We compare the richness for the different luminosity cuts relative to this value using the bootstrap resampling method, and find that the proposed cut of $0.2L_*$ is significantly (5σ) better than the original luminosity cutoff of $0.4L_*$. The resulting scatter value is $\sigma_{\ln L_X|\lambda} = 0.63 \pm 0.02$, with a corresponding redshift evolution parameter of $\gamma = 0.6 \pm 0.5$, consistent with both no evolution and self-similar evolution.

One question that may arise from looking at Figure 2 is whether the flattening in the scatter as a function of luminosity cut is driven by the fact that by $L_{cut} = 0.1L_*$ one begins to approach the limiting magnitude of the SDSS galaxy catalog for galaxies at $z = 0.3$. To test this hypothesis, we have run the same scatter analysis on the lower redshift half of our cluster sample, i.e., clusters with redshift below the median redshift of the sample, $z_{\text{med}} < 0.23$. We maintain the same equivalent space-density cutoff as the full run (black diamonds) by limiting the scatter measurement to the top 1000 clusters. The resulting points are shown in Figure 2 as red squares, and clearly display the same behavior as the full cluster catalog. At $z = 0.23$, a luminosity of $0.2L_*$ ($0.1L_*$) corresponds to $i = 19.9$ (20.7), significantly brighter than the limiting magnitude of the catalog. Thus, we can only conclude that the flattening of the scatter below $0.2L_*$ is real, and not due to photometric errors of faint galaxies.

¹⁹ Note that in principle one could measure distances to the perpendicularly to the ridgeline, as opposed to along the color axis as we have done. Fortunately, the fact that the tilt of the red-sequence is small implies that we do not expect such differences to be significant.

²⁰ See Section 3.2 for details on the calculation of L_* .

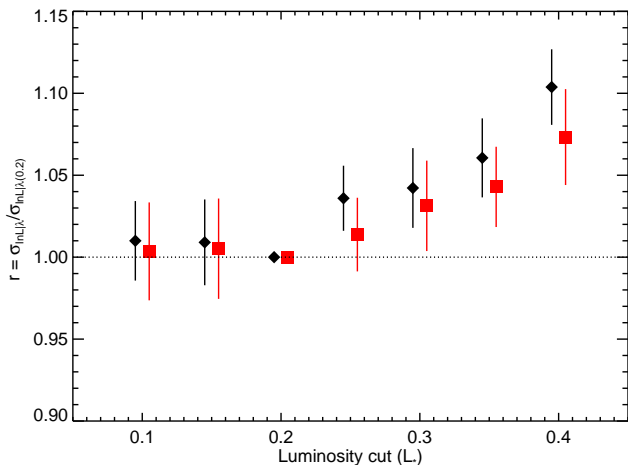


FIG. 2.— Comparison of the scatter in L_X at fixed richness for a set of luminosity cuts. To assess the significance of the improvement, each richness scatter, $\sigma_{\ln L_X|\lambda}$ is compared via the bootstrap resampling method to the scatter measured with a luminosity cutoff of $0.2L_*$, $\sigma_{\ln L_X|\lambda(0.2)}$. The black diamonds show the results for the full cluster sample, and the red squares for the lower redshift clusters with $z < 0.23$. In both cases the scatter decreases until a luminosity cutoff of $0.2L_*$, and does not improve with deeper observations. Note that the comparison of λ at $0.2L_*$ to itself is identically 1.

For the time being, we simply adopt this new optimal luminosity cut, postponing the discussion of the origin of this cut to Section 6. For reference, decreasing our luminosity cut from $0.4L_*$ to $0.2L_*$ increases the cluster richness by an average of $\approx 65\%$.

4.5. Radial Filter

The NFW profile was originally introduced as a good fit for the dark matter distribution in N-body simulations (Navarro et al. 1995). Although galaxies will not necessarily follow the same distribution as that of dark matter, studies have shown that the number density of cluster galaxies can be described by an NFW function (e.g. Lin & Mohr 2004; Popesso et al. 2007; Hansen et al. 2005). Nevertheless, a filter based on an NFW profile might not necessarily be ideal. In this section we investigate the effect of changing the radial filter function.

A projected NFW profile extends to infinity, so we are required to normalize the filter taking into account the cutoff radius. An alternative radial profile suggested by Postman et al. (1996) instead goes to zero at the cutoff radius:

$$\Sigma_{\text{post}}(R/R_{\text{core}}) \propto \frac{1}{\sqrt{1 + (R/R_{\text{core}})^2}} - \frac{1}{\sqrt{1 + (R_c/R_{\text{core}})^2}}. \quad (25)$$

The equation assumes $R < R_c$, where R_c is the cluster radius as defined in Eqn. 4; outside of this radius, $P = 0$. We follow Postman et al. (1996) in setting $R_{\text{core}} = 100 h^{-1} \text{ kpc}$, and we normalize the filter as in Eqn. 8. This profile gives more weight to the central galaxies and less weight to the peripheral galaxies than the NFW filter. We denote the resulting richness, λ_{post} .

Finally, we also investigate a third possibility, that of replacing the radial filter $2\pi R\Sigma(R)$ with a flat top-hat function, i.e. $\Sigma(R) \propto 1/R$ or isothermal, which defines λ_{flat} . This gives equal weight to cluster galaxies at the center and those at the periphery.

We perform a pairwise comparison of the scatter in L_X at fixed richness among our three richness estimators generated with three radial functions, λ_{NFW} , λ_{post} , and λ_{flat} . For these tests, we use the best luminosity cutoff ($0.2L_*$), the color filter including tilt, and fix the cutoff radius at $0.9 h^{-1} \text{ Mpc}$. In the comparison of the flat profile to the NFW profile, we find $r = \sigma_{L_X|\lambda_{\text{flat}}}/\sigma_{L_X|\lambda_{\text{NFW}}} = 1.03 \pm 0.015$. Thus, using the NFW profile is better than using a flat radial profile at the 2σ level. Comparing the Postman profile to the NFW profile, we find $r = \sigma_{L_X|\lambda_{\text{post}}}/\sigma_{L_X|\lambda_{\text{NFW}}} = 1.016 \pm 0.016$.

The NFW profile gives slightly more weight to peripheral cluster galaxies than the Postman filter, and less weight to the peripheral galaxies than the flat filter. The NFW filter, somewhere in the middle, narrowly outperforms the other two, which are closer to the extremes. That said, it is worth noting that up to $\approx 30\%$ number of BCGs in the maxBCG catalog may not be at the halo center (Johnston et al. 2007). Therefore, we cannot rule out the possibility that our results are driven at least in part by miscentering inherent to the maxBCG catalog. Nevertheless, our tests in this section show that the shape of the radial profile has a relatively *weak effect* on the fidelity of the richness estimator λ . Thus, we do not feel it is necessary to expend further energy in exploring a broad variety of possible radial filter functions.

4.6. Luminosity Weighting

Total optical luminosity of a cluster has been suggested as a superior mass tracer to simply galaxy counting (e.g. Popesso et al. 2005, and others), though any such improvement is likely to be small as the optical luminosity and total number of cluster galaxies are highly correlated (e.g. Popesso et al. 2005, 2007; Koester et al. 2007a). In this section we explore this possibility by using the total optical luminosity of red sequence galaxies in clusters as an X-ray luminosity tracer.

We have already seen that our λ formalism naturally produces a red-sequence based cluster membership probability. Consequently, we can readily estimate the total red-sequence cluster luminosity L_λ via

$$L_\lambda = \sum_j L_j p_j, \quad (26)$$

where L_λ is the luminosity weighted lambda, p_j is the membership probability of galaxy j , and L_j is the luminosity of galaxy j . The luminosity is defined as the i -band luminosity of a galaxy at $z = 0.25$, and all galaxies are k -corrected assuming the galaxies are red galaxies at the redshift of the cluster. We calculated L_λ for our clusters using the the best luminosity cutoff ($0.2L_*$), the color filter including tilt, and with a fixed $0.9 h^{-1} \text{ Mpc}$ aperture. We find a scatter of $\sigma_{\ln L_X|L_\lambda} = 0.68 \pm 0.02$, and a redshift evolution parameter $\gamma = -1.0 \pm 0.6$. The bootstrap comparison to the corresponding λ estimate results in $r = \sigma_{\ln L_X|L_\lambda}/\sigma_{\ln L_X|\lambda} = 1.09 \pm 0.02$. Thus, calculating the red-sequence luminosity of the clusters is a *worse* tracer of L_X than pure red-sequence counts.

One worry when interpreting this results is that the result may be systematics driven. Specifically, in estimating the cluster luminosity we assume all galaxies are at the cluster redshift, which can dramatically boost the luminosity assigned to any foreground galaxies. Even with low membership probabilities, such boosts might significantly bias the estimated cluster luminosity. To test this hypothesis, we have repeated our experiment while restricting the sum in Eqn. 26 to galaxies fainter than the BCG. We find that our results are robust to this change, which suggests foreground interlopers are not the culprit. There is the additional possibility that the more numerous faint galaxies, with larger photometric errors, are increasing the noise. However, the same trend — that simple number counts are superior to luminosity weights — appears with richnesses using brighter luminosity cuts. Thus, we conclude that the total red-sequence cluster luminosity is a *worse* L_X tracer than red-sequence galaxy counts.

Another type of luminosity weighting that has been suggested in the past is weighting by the luminosity of the BCG (e.g. Reyes et al. 2008). In Paper I, we showed that the richness estimate of Reyes et al. (2008), while superior to N_{200} , has a significantly larger scatter than λ_0 . Similarly, in the present work we did not observe any significant difference when combining λ with the BCG luminosity. This may be simply a fact that our tests are primarily focused on the high richness end. It is clear that at sufficiently low richness — e.g., $\lambda = 1$, or a single red galaxy — the luminosity of the BCG must contain additional information about the mass of the host halo. We emphasize that these results do not contradict those of Reyes et al. (2008). The reason is that although significant improvements can be made relative to N_{200} , these are not as easily achieved relative to our optimized λ richness estimator.

4.7. Aperture Optimization

Having explored ways in which λ could be improved while relying on a fixed metric aperture, we now turn towards optimizing cluster radii. Throughout this section, we use our final set of filters, given by

$$u(c, m, r|z, \lambda) = [2\pi R \Sigma(R)] \phi(m) G(c, m), \quad (27)$$

where $\Sigma(R)$ is given by Eqn. 6, $\phi(m)$ is given by Eqn. 10, and $G(c, m)$ is given by Eqn. 21. In addition, our luminosity filter now extends to a luminosity cutoff $L_{\text{cut}} = 0.2L_*$. For the rest of this paper, we denote the matched filter richness estimate from this filter simply as λ . We proceed now to optimize the radial scaling parameters R_0 and β from Eqn. 4.

We optimize the radial aperture using the procedure laid out in detail in Paper I. Briefly, we begin by defining a coarse grid in R_0 and β , and estimate the scatter $\sigma_{\ln L_X|\lambda}$ along this grid. Once we have a rough idea of where the minimum lies in parameter space, we repeat this search using a finer grid centered on the expected minimum. We then use bootstrap resampling to estimate the 1σ and 2σ confidence contours of the location of the scatter minimum in the $R_0 - \beta$ plane. For a more detailed description of this algorithm, we refer the reader to Section 4 of Paper I.

Figure 3 shows our final set of contours. The minimum on the fine grid is consistent with the coarse grid,

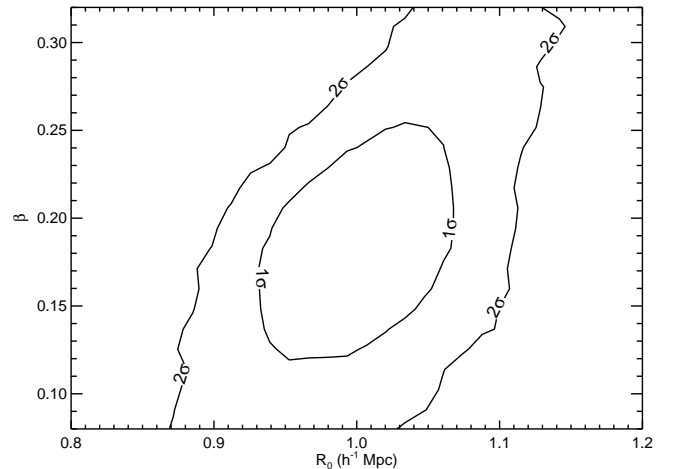


FIG. 3.— Contours of the probability density of the location of the point in the $R_0 - \beta$ plane that minimizes the scatter in L_X at fixed richness. The lines show the 1σ and 2σ contours. In the interest of simplicity, we choose as our final fiducial parameters $R_0 = 1.0 h^{-1} \text{Mpc}$ and $\beta = 0.2$ in the scaling relation $R_c = R_0(\lambda/100)^\beta$, which are consistent with the minimum scatter. We note that these parameters yield $R_c \sim 0.9 h^{-1} \text{Mpc}$ for a cluster with $\lambda = 45$, the median richness of the richest 2000 clusters, and thus the reference aperture of $0.9 h^{-1} \text{Mpc}$ is consistent with the scaled aperture.

with radial scaling parameters of $R_0 = 1.0 h^{-1} \text{Mpc}$ and $\beta = 0.2$ for use in the scaling relation $R_c = R_0(\lambda/100)^\beta$. These values are in good agreement with the trends seen in Paper I. Although the 1σ contour is closed, there is a broad degeneracy region that extends down to a fixed metric aperture with $R_0 = 0.9 h^{-1} \text{Mpc}$ and $\beta = 0.0$. In particular, for a cluster with $\lambda = 45$, the median richness of the richest 2000 clusters, the scaled aperture is $\sim 0.9 h^{-1} \text{Mpc}$. Therefore the reference fixed aperture of $0.9 h^{-1} \text{Mpc}$ is consistent with the scaled aperture, and the richness comparisons in the previous sections are indeed valid for our final richness estimator. However, as discussed in Paper I, the existence of the degeneracy line shown in Figure 3 is largely driven by the limited richness range that we can probe using X-ray luminosity. We fully expect the variable aperture approach is superior to a fixed metric aperture, particularly when probing lower richness systems, although those systems are out of reach for our present analysis.

For the radial scaling parameters of $R_0 = 1.0 h^{-1} \text{Mpc}$ and $\beta = 0.2$ used in the final version of λ , the scatter in L_X for the top 2000 clusters is $\sigma_{\ln L_X|\lambda} = 0.63 \pm 0.02$, and the evolution parameter is $\gamma = 0.5 \pm 0.5$. These values are consistent with those estimated for the fixed $0.9 h^{-1} \text{Mpc}$ aperture, and the relative improvement is not significant, with $r = 0.99 \pm 0.02$.

5. SYSTEMATICS

In this section, we discuss several sources of systematic error that may have an effect on the calculation of the λ richness estimator. Our goal is to show that our method is particularly robust to common perturbations, and furthermore will produce consistent results even when we are not using SDSS data. In particular, in Section 5.1

we explore how λ changes if alternative filters are used to isolate the red sequence. In Section 5.2 we look at the effect of the normalization of the global background. In Section 5.3 we look at variations in the width of the red sequence in the model, and in Section 5.4 we look at the effect of uncertainty in the photometric zero-point. In Section 5.5 we investigate the effects on the calculation of λ if we do not know the color–redshift relation. Finally, in Section 5.6, we determine the effect of “catalog noise,” false galaxies that add noise to the input galaxy catalog.

5.1. The Robustness of λ to the Choice of Filters

Up until now, we have focused our analysis on the color–magnitude relation as described by $g - r$ v. i . As discussed above, the $g - r$ color is well suited for cluster photometric redshift and richness estimation in the $0.1 < z < 0.3$ range covered by the maxBCG catalog. However, this filter combination is not uniquely able to isolate the cluster red sequence and evolve smoothly with redshift. In order for the richness estimator λ to be generally useful, and to be extended to higher redshifts, it must be robust to changes in filters. In this section we use additional SDSS data to investigate how λ changes with alternative filter choices.

We have chosen to focus our analysis on three alternative color combinations: $g - i$, $r - i$, and $u - r$. Three bands — g , r , and i — have high quantum efficiency in SDSS, and thus we do not need to worry about significant problems with photometry near the limiting magnitude. When using the u band data we limit the redshift range to $z < 0.25$ (see below). The colors $g - i$ and $u - r$ have the advantage of containing the g band which changes strongly as the 4000 Å break moves with redshift. Although the $r - i$ color evolves with redshift and allows us to pick out the red sequence, this evolution is not as strong as when combined with the g color, and thus we expect that λ may not perform as well.

To create the red sequence model of the filter, we follow the method of Hao et al. (2009, see Section 5.1). For each cluster with $\lambda_0 > 10$ we take all galaxies within $0.9 h^{-1}$ Mpc and brighter than $0.4 L_*$. We use the error-corrected Gaussian mixture model to decompose the red sequence and blue cloud/background for the color of interest. We then fit a linear model to all galaxies with $\pm 2\sigma$ of the red sequence, yielding a slope and intercept at $i = 17$, m_{17} and b_{17} (as in Section 4.3). Next we bin the clusters in redshift bins of width 0.02 and calculate the mean $\langle m_{17} \rangle$ and $\langle b_{17} \rangle$. Finally, we fit a linear model as a function of redshift to obtain a simple functional form of $\langle m_{17} | z \rangle$ and $\langle b_{17} | z \rangle$ akin to Eqn. 23. This model is used to calculate the given richness within a fixed metric aperture of $0.9 h^{-1}$ Mpc.

Figure 4 shows the comparison of λ calculated with various color filters to the basic λ_{g-r} . In the top panel we compare λ_{g-i} , in the middle panel we compare λ_{r-i} , and in the bottom panel we show λ_{u-r} . The top two panels show all maxBCG clusters, and the bottom panel only those with $z < 0.25$ due to the smaller sensitivity in the u band. The inset histograms illustrate the distribution of differences between the given richness and λ_{g-r} .

Table 1 shows the results of comparing the richness estimates to the baseline λ_{g-r} . First, we have estimated the width of the distribution, $\Delta\lambda_{\text{rms}}$, shown in the in-

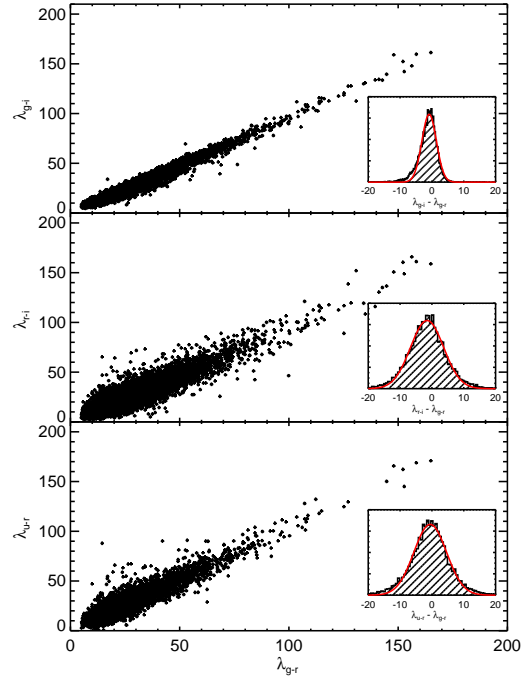


FIG. 4.— Comparison of λ calculated with different filter combinations, and compared to the basic λ_{g-r} . In the top panel is λ_{g-i} , in the middle panel is λ_{r-i} , and in the bottom panel is λ_{u-r} . The inset histograms illustrate the distribution of $\delta = \lambda_{\text{alternate}} - \lambda_{g-r}$. Changing from the $g - r$ color to the $g - i$ color does not have a significant effect on the richness estimation.

TABLE 1. COMPARISON OF RICHNESSES TO BENCHMARK λ_{g-r}

Richness	$\Delta\lambda$	r
λ_{g-i}	-0.9 ± 2.3	1.01 ± 0.01
λ_{r-i}	-1.5 ± 5.2	1.11 ± 0.03
λ_{u-r}	-0.5 ± 5.1	1.12 ± 0.03

NOTE. — All richnesses are measured in a fixed metric aperture of $0.9 h^{-1}$ Mpc. $\Delta\lambda$ shows the change relative to the benchmark λ_{g-r} .

set plots of Figure 4. We report $\Delta\lambda$ rather than $\Delta\lambda/\lambda$ because it is the former that is roughly constant with richness. Second, we have compared the scatter in $\sigma_{L_X|\lambda}$ using the bootstrap resampling ratio r described in Section 4.1. For the first two alternative versions of λ we use the top 2000 clusters in the full redshift range; for λ_{u-r} we use the top 1000 clusters for the lower redshift range $0.1 < z < 0.25$.

It is readily apparent that the change from λ_{g-r} to λ_{g-i} is nearly insignificant. The median richness of the top 2000 clusters is ~ 45 , so the observed scatter is $\lesssim 4\%$. For reference, Poisson scatter at this richness would correspond to $\approx 15\%$ scatter, while Rozo et al. (2010a) estimate the scatter in N_{200} at fixed mass to be $\approx 35\%$. In short, $g - i$ is effectively as efficient as $g - r$ for the purposes of selecting red-sequence galaxies, reflecting the fact that the 4000 Å break falls within the g filter.

Focusing now on the $r - i$ and $u - r$ filter combinations, we see these choices exhibit a significantly larger scatter

in $\Delta\lambda$, of order 10%, still less than Poisson scatter, and much less than the Rozo et al. (2010a) estimate for N_{200} . This increased scatter relative to $g-r$ is also reflected as increased scatter in L_X at fixed richness. In the case of $r-i$, this can be understood by the fact that our filter combination does not straddle the 4000 Å break, and therefore the red sequence is not as prominent against the background. The $u-r$ color does straddle the 4000 Å break, but suffers from the much lower SDSS sensitivity in the u band.

In summary, we see that an effective use of the λ richness does not require the specific $g-r$ filter combination used in this work. Indeed, use of *any filter combination that can effectively isolate the red-sequence will result in nearly identical and unbiased values for λ* , although the scatter is reduced when using high sensitivity filters that straddle the 4000 Å break. Even in the case of the less optimal $r-i$ and $u-r$ combinations we get a reasonable, although not ideal, richness estimator. Due to the stability of λ when using different filter combinations, we expect these methods to be easily generalizable for other telescopes and higher redshifts.

5.2. Background Normalization

With the entire SDSS DR7 at our disposal, covering ~ 7500 square degrees, we can make a very accurate estimation of the global background as a function of color and magnitude. In other instances, however, there may be greater uncertainties in the true mean background for a given filter combination. In this section we investigate the effect of varying the background level on λ .

In general, uncertainties in the background will be a function of color and magnitude. For simplicity, we model uncertainty in the background as a boosting or de-boosting of the background normalization. Our intention with this approximation is to give a rough estimate of the systematic uncertainty in richness estimates given the uncertainty in the background. We expect that a boost of the background normalization $b(\mathbf{x})$ will cause the richness λ to decrease by a fixed amount (independent of λ) and a decrease of the background normalization will cause λ to increase by a similar amount.

In Figure 5 we show the effect of changing the background normalization on the calculation of λ in a fixed $0.9 h^{-1}$ Mpc aperture. When the background normalization is deboosted by a factor of 0.5, then λ changes by $\Delta\lambda = 6.6 \pm 2.9$, and when it is boosted by a factor of 1.5, then $\Delta\lambda = -4.2 \pm 1.7$. For a moderate richness cluster of $\lambda \sim 30$, incorrectly estimating the background by $\sim 50\%$ can bias the richness by $\sim 20\%$, approximately equal to the Poisson scatter. On the other hand, a $\sim 10\%$ error in the background normalization has a negligible effect on the richness estimation of $\sim 3\%$. We emphasize these values are only meant to help in estimating how precisely the background must be modeled in order to ensure a negligible impact on richness estimates.

5.3. Red Sequence Width

In our adapted color filter from Section 4.3, and in all our tests, we fix the intrinsic scatter in the red sequence at $\sigma_{\text{int}} = 0.05$. We now investigate the effect on λ and $\sigma_{L_X|\lambda}$ on changes in the intrinsic scatter, similar to the tests of Section 4.3 in Paper II. For this test, we fixed the radial size at $0.9 h^{-1}$ Mpc, and set the red sequence

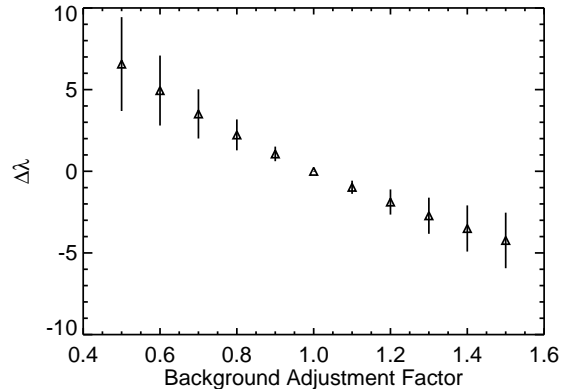


FIG. 5.— Change in λ ($\Delta\lambda$) as a function of background adjustment factor. When the background normalization is deboosted by a factor of 0.5, the richness estimate changes by $\Delta\lambda = 6.6 \pm 2.9$, and when it is boosted by a factor of 1.5, then $\Delta\lambda = -4.2 \pm 1.7$. If one knows the background normalization to $\sim 10\%$ then the bias in the richness estimation is less than the statistical error.

width to 0.03 mag and 0.07 mag, representing a narrow and wide extreme.

In each case, we find that the effect on both the scatter and the richness estimate is negligible. For $\sigma_{\text{int}} = 0.05$, then $\Delta\lambda = -1.5 \pm 1.0$ and for $\sigma_{\text{int}} = 0.07$, then $\Delta\lambda = 1.2 \pm 0.9$. Unsurprisingly, if we take a narrower (wider) red sequence then the richness estimate decreases (increases) as we lose (gain) galaxies at the margins. However, the total probability of these additional galaxies is quite small, and the overall bias in the richness estimate is negligible. Note that one reason that λ is not very sensitive to the red sequence width is because the color filter in Eqn. 12 uses the sum in quadrature of the photometric error and intrinsic color dispersion. We conclude that our richness estimator is robust to changes in the red sequence width, and thus is suitable for other filter combinations that span the 4000Å break that may have slightly different ridgeline widths.

5.4. Zero-Point Uncertainty

The calculation of λ requires measuring all the galaxies above a given luminosity threshold that evolves with redshift. In practice, uncertainty in the luminosity threshold is equivalent to uncertainty in the photometric zero-point as well as systematic offsets in differing methods of calculating galaxy magnitudes. In this section we explore the effect of an offset in the photometric zero-point, which is equivalent to each of these effects.

As before, we run with a fixed $0.9 h^{-1}$ Mpc aperture with a range of systematic offsets in the magnitude limit for the luminosity function filter (Eqn. 10). We find that for small zero-point shifts – up to ± 0.05 mag – the effect on λ is negligible ($\delta\lambda < 1$) for the vast majority of clusters, consistent with the observation in Paper II that such errors do not significantly impact the scatter of the richness–mass relation. This is because only rarely is a red sequence galaxy added or removed from consideration when making such a small shift. Of course, large photometric shifts in rich clusters can be significant. For instance, a ± 0.1 mag shift in a rich cluster can change λ

by $\approx 10\%$. Note, however, that such photometric errors are much larger than expected for upcoming photometric surveys.

5.5. Uncertainty in the Color-Redshift Relation

In this section we investigate the effect of uncertainty in the color-redshift relation for the Gaussian color filter. If we were to follow the strategy of the preceding sections, we would approach this issue by systematically shifting the slope and intercept of the color filter. However, this treatment would unrealistically ignore the data at hand. When observing an actual galaxy cluster, we can always *measure* the red sequence for each individual cluster. Therefore, we explore the effect on λ if we measure the red sequence intercept and slope for each cluster individually.

For each maxBCG cluster, we first take all the galaxies within $0.9 h^{-1}$ Mpc and brighter than $0.2L_*$. To measure the intercept and slope of the red sequence, we follow the method of Sections 4.2 and 4.3. The color distribution of galaxies is decomposed into two Gaussians (the red sequence and the blue/background galaxies) using the Error Corrected Gaussian Mixture Model of Hao et al. (2009). To limit the degrees of freedom to allow for accurate fitting of relatively poor clusters ($\lambda \lesssim 30$), we fix the width of the red sequence component at $\sigma_{\text{int}} = 0.05$ mag. One could in principle also attempt to fit this from the data, but we have already shown that the recovered richness is largely insensitive to this parameter, and the typical ridgeline width is ≈ 0.05 . If the mixture model is unable to identify two distinct components then the cluster is flagged and λ is not measured. We then take all galaxies within $2\sigma_{\text{int}}$ and fit the red sequence slope and intercept. These values are then substituted for Eqn 23 to calculate the richness λ .

Figure 6 shows the comparison of λ_{fit} , where we fit for the red sequence on a cluster-by-cluster basis, to λ in a fixed $0.9 h^{-1}$ Mpc aperture. Results are nearly identical with a variable aperture with $R_0 = 1.0 h^{-1}$ Mpc and $\beta = 0.2$. The inset plot shows that for individual clusters λ shifts by a negligible 0.1 ± 0.6 . Overall, the richness measurement is extremely robust to perturbations in the red sequence location. This is due to a combination of the contrast of the red sequence with the background galaxies, and the fact that the smooth Gaussian color filter is more tolerant of color offsets than a top-hat filter (as explored in Section 6 of Paper I). It should be noted that our automated algorithm for red-sequence fitting succeeded in measuring the red-sequence for all clusters of richness $\lambda \gtrsim 50$. At $\lambda \leq 40$, the failure rate was $\approx 10\%$. We are confident that this failure rate could be decreased if one incorporated even mild priors on the red-sequence parameters, for instance from population synthesis models. The main point here is not the automated red-sequence fitting, but rather the fact that so long as the red-sequence can be properly fit from the data, one does not need an a-priori model for the red-sequence in order to be able to compute λ . Of course, having such a model will help in the limit of low signal-to-noise, and is less computationally intensive.

5.6. Catalog Noise

As discussed in Section 2.3, a clean input catalog is required for accurate cluster finding and richness estima-

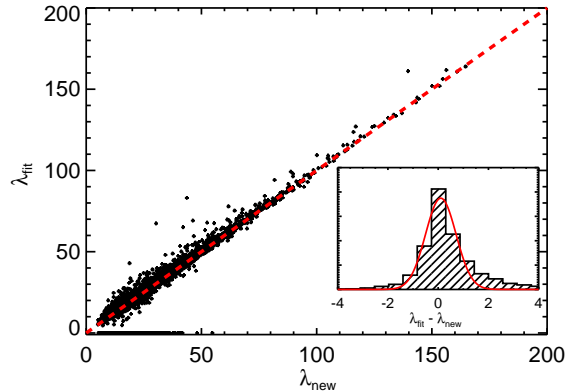


FIG. 6.— Plot of λ_{fit} , using the red sequence fit for each individual cluster, against λ , our optimized richness, with a fixed $0.9 h^{-1}$ Mpc aperture. The inset shows the histogram of $\Delta\lambda$, which has a negligible offset and scatter of 0.1 ± 0.6 . However, at $\lambda < 40$, about 10% of the clusters are not measured as we were unable to properly decompose the red sequence component from the background using the ECGMM method.

tion. The old mantra “garbage in, garbage out” is especially apt. We refer to the inclusion of any object that is not a correctly measured galaxy as “catalog noise.” This includes stars, asteroids, image artifacts, and improperly measured photometric errors. In general, it also includes pipeline-to-pipeline variations in the reduction, detection, and photometry for the same object. In this section, we obtain a first-order estimate of the magnitude of the effect of catalog noise on our richness estimation.

To test the effect of catalog noise, we compare the scatter in L_X at fixed richness for two versions of the input catalog. The first is the “clean catalog” that has been filtered as described in Section 2.3. The second is the raw catalog, using all the objects marked as galaxies in DR7 without any additional filtering. Figure 7 shows the histogram of the number of objects as a function of i -band magnitude for stripe 10 in SDSS. There are significantly more galaxies at the faint end in the uncleaned catalog (red dashed histogram), many of which are false detections.

For each input galaxy catalog, we first compute the background as described in Section 3.4. We then compute both λ_0 , the original matched filter richness, and λ , the optimized richness, both at the fiducial fixed $0.9 h^{-1}$ Mpc scale. We expect that the effect of catalog noise will be greater on λ , as it uses a deeper luminosity cut where the catalog noise is greater. This is indeed what we find for the top 2000 clusters, where the scatter in the L_X at fixed richness increases from 0.70 ± 0.02 to 0.72 ± 0.02 for λ_0 , and from 0.63 ± 0.02 to 0.66 ± 0.02 for λ . Using the bootstrap resampling ratio r described in Section 4.1, we find that using the noisy catalog increases the scatter by $r = 1.03 \pm 0.02$ for λ_0 and $r = 1.04 \pm 0.02$ for λ . In addition, we confirm that the scatter measured is consistent between the cleaned DR7 catalog and the cleaned DR4 catalog used in Paper I. Thus, at least for different versions of the SDSS pipeline λ is robust to this level of pipeline-to-pipeline variations.

Overall, with our current catalog and our best richness

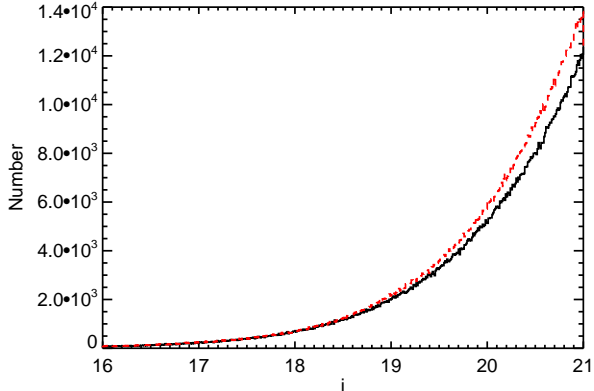


FIG. 7.— Histogram of number of galaxies in SDSS stripe 10 from DR7. The solid black histogram shows the galaxies as a function of i -band magnitude for the clean input catalog as described in Section 2.3. The dashed red histogram shows the raw input catalog from DR7, without the additional flag cuts. There are significantly more galaxies at the faint end, most of which are false detections.

estimator, we can detect the effect of catalog noise at the 2σ level in our chosen figure of merit. Therefore, catalog noise is a nuisance, though it is not a critical path item. This is partly due to the high quality of the raw SDSS DR7 catalog. However, we emphasize that we can detect this effect even though we are recomputing the background for each input catalog, and these false galaxies are presumably not correlated with the cluster positions. Thus, increased noise in the background does translate to increased scatter in the richness estimator, and should be controlled as well as possible.

6. THE ORIGIN OF THE OPTIMAL RADIAL AND LUMINOSITY CUTS

We have demonstrated the existence of optimal radial and luminosity cuts when evaluating the richness of maxBCG galaxy clusters. We have not yet, however, offered an explanation for the origin of these cuts. Indeed, in a naive Poisson scatter model outlined in Paper II, one should expect larger apertures and fainter magnitude cuts to *always* result in reduced scatter simply due to the larger galaxy count. What then changes these conclusions?

We address these questions by relying on the simulation method from Paper II, which we now briefly summarize. We model galaxy clusters using an NFW profile, with a Schechter luminosity function, and a Gaussian color distribution. Each cluster realization is then embedded in a realization of a uniform density field meant to represent the local galaxy background. The background density field can be set to the mean galaxy density of the universe, which we refer to as uniform background, or it can be modeled so as to match both the mean and variance of the local density field around SDSS maxBCG galaxy clusters. We refer to this latter model as the random background model, since each cluster is embedded in a different background.

There were two key insights from Paper II that are relevant for this discussion. The first is that the scatter in richness at fixed mass depends sensitively on miscentering parameters. Indeed, Paper II concludes that the

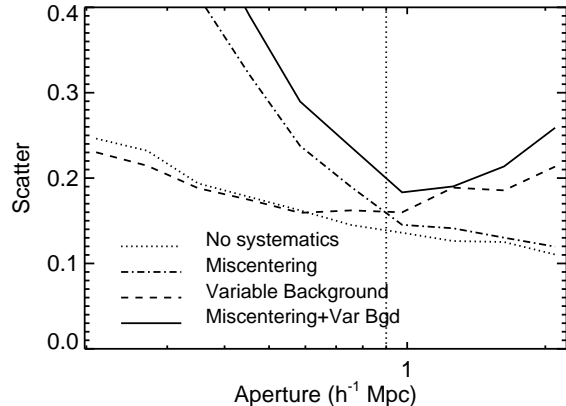


FIG. 8.— The scatter in richness at fixed mass in our Monte Carlo simulations for four different models, as labeled (see text for details on the models). We see that miscentering creates a floor below which the scatter increases rapidly, while projection effects in the realistic random background model (chosen to match SDSS data) pushes the optimal aperture inward. Thus, the optimal aperture reflects a compromise between these two sources of error. Note that even without miscentering we find an optimal aperture using the variable background model. The vertical dotted line is the optimal aperture from section 4.7.

scatter for maxBCG clusters is dominated by miscentering. The second key insight concerns the local galaxy background within which clusters are embedded. Specifically, we find that the majority of clusters are embedded in a low density background, with 1%–5% of the clusters embedded in high density backgrounds that results in a severe over-estimate of the clusters’ richness. These rare occurrences were interpreted as the signature of projection effects in CDM cosmologies.

Given these two key insights, we consider whether these two effects — miscentering and the stochastic nature of the background galaxy density — give rise to the optimal aperture and luminosity cuts we have uncovered empirically. To do so, we perform Monte Carlo realizations of galaxy clusters with four different models:

1. No systematics (no variable background; no miscentering)
2. Miscentering (no variable background)
3. Variable background (no miscentering)
4. Miscentering and variable background

For each of these four models, we generate between 400 and 5000 Monte Carlo realizations of galaxy clusters²¹, and then measure the richness using a variety of radial aperture and luminosity cuts. This data is then used to estimate the scatter in richness, which we plot as a function of the radial and aperture cuts.

Figure 8 shows how the scatter in richness at fixed mass varies for each of the four models detailed above. For models with miscentering, we assumed 80% of the clusters are centered correctly, while the remaining 20% are radially offset by first picking a random axis, and

²¹ See Paper II for details on the construction of the realizations

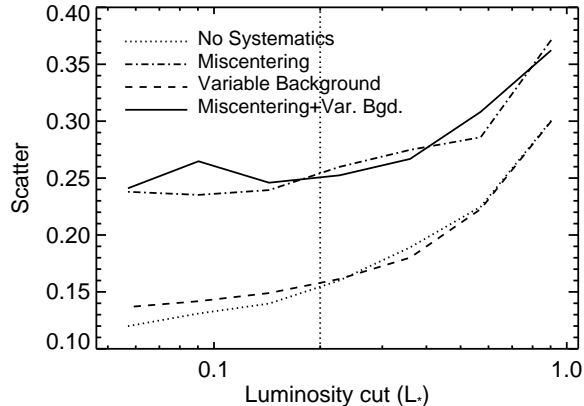


FIG. 9.— The scatter in richness at fixed mass in our Monte Carlo simulations for four different models, as labeled (see text for details on the models). In miscentering models, lowering the luminosity cut tends to lower the scatter, but only up to a point. The vertical dotted line in the figure is the luminosity cut below which we did not see any significant improvement in the data. Thus, it is likely that the flattening of the luminosity scatter in Figure 2 primarily reflects the miscentering properties of the maxBCG catalog.

then displacing along this axis by randomly drawing from a Gaussian of mean zero, and standard deviation $\sigma = 0.4 h^{-1}$ Mpc (e.g., Johnston et al. 2007). The vertical dotted line is the optimal fixed metric aperture of $0.9 h^{-1}$ Mpc that we found in the data. Not surprisingly, miscentering requires that the optimal aperture be significantly larger than the miscentering kernel, creating an aperture floor below which the scatter increases rapidly. In the other direction, moving outward is penalized when estimating the richness of clusters in the (realistic) random background model. This is easy to understand: if the background density is high, the larger the aperture, the larger the noise in the richness estimate of those clusters suffering from projection effects. The optimal aperture is therefore a compromise between these two sources of stochasticity. Note, however, that even without miscentering we find an optimal aperture using the variable background model, which simply reflects the fact that as the aperture goes to zero, the scatter necessarily increases since there are fewer cluster galaxies.

Figure 9 illustrates how the scatter in richness at fixed mass varies in our Monte Carlo simulation as a function of the luminosity cut employed when estimating cluster richness. The vertical dotted line corresponds to the optimal luminosity cut from section 4.4. Even in the absence of miscentering, it can be seen that the gains when using a deeper luminosity threshold than $0.2L_*$ are marginal. However, miscentering introduces an additional “scatter floor,” and once this floor is reached, reduction in the scatter is no longer possible. We expect that when using cluster catalogs with improved centering properties further reduction in the scatter should be possible. Additional gains may be made by lowering the luminosity threshold L_{cut} , although the rate of improvements is rather low. Of course, at some point a new scatter floor has to arise from other effects (e.g. triaxiality), but these effects are not dominant in the maxBCG catalog if the

miscentering model of Johnston et al. (2007) is correct.

7. SUMMARY AND CONCLUSIONS

In this paper, we have shown the improvements in the matched filter richness estimator presented in Paper I. By gauging improvement by the decrease in scatter in X-ray luminosity at fixed richness, we can quantitatively determine which optical proxies are superior as a tracer of halo mass. Our final optimized richness λ uses a probabilistic formalism to estimate the number of red sequence galaxies brighter than $0.2L_*$ in the cluster. We emphasize that our goal is to find a high fidelity mass tracer, and we leave an analysis of the complete census of cluster galaxies to separate work (e.g., Hansen et al. 2009).

Relative to the matched filter richness described in Paper I we find:

1. Lowering the luminosity threshold results in decreased scatter, but only as far as $0.2L_*$. Using Monte Carlo simulations, we show that this limit is partially driven by the miscentering properties of the maxBCG catalog. Consequently, catalogs with improved centering properties may benefit from going even deeper. However, even without miscentering, the rate at which the scatter is reduced is rather modest, so such benefits are likely to be limited.
2. Modifying the color filter to account for the blue galaxy population (which makes up $\gtrsim 20\%$ of the galaxy population) results in increased scatter. We are unable to determine whether the increased scatter is intrinsic (e.g., the blue galaxies have more recently fallen into the cluster), or if it is simply caused by the fact that the blue galaxies are much less prominent against the background, yielding a noisy measurement. Either way, generalizing color filters to include blue galaxies is inadvisable for photometric catalogs.
3. Weighting each galaxy by its luminosity results in increased scatter, and weighting each cluster by the BCG luminosity (e.g., Reyes et al. 2008) does not improve the scatter. However, our tests only probe the high richness end, and the possibility of further improvements at low richness, where the luminosity of the BCG is more dominant, are not ruled out.
4. Incorporating red sequence tilt does not have a measurable impact on the recovered scatter. Nevertheless, we have modified our estimator to include this tilt, both because it may become relevant for fainter luminosity cuts, and because we expect the tilt to become more important at higher redshifts with different filter combinations.

Following Paper I, we also optimized the radial aperture used to estimate cluster richness. Our best fixed metric aperture is $0.9 h^{-1}$ Mpc, though we expect scaled apertures should be better due to the standard “bigger things are bigger” maxim. Assuming a power-law relation between radial cutoff and cluster richness, we find that $R_c = 1.0(\lambda/100)^{0.2} h^{-1}$ Mpc. Although we cannot test the scaling relation at low richness, we expect the

scaled aperture to be superior to the fixed metric aperture further down the richness function. Following Paper II, we used Monte Carlo simulations to demonstrate that the optimal aperture we have measured reflects a compromise between cluster miscentering and projection effects; cluster miscentering creates a hard floor on the minimal aperture, while projection effects push towards smaller apertures. Even in the absence of miscentering, simple counting statistics (smaller apertures find fewer galaxies) combined with projection effects would yield a similar optimized aperture. We also investigated whether the shape of the radial filter can result in improved richness estimators, but found that the detailed shape of this filter has only a very modest impact on the recovered scatter.

Our work is most comparable to that done using the X-ray selected RASS–SDSS galaxy cluster catalog (Popesso et al. 2004), who first explored the idea of using X-ray data to improve and calibrate optical richness/luminosity estimators. Popesso et al. (2004) found an optimal aperture significantly smaller than the $\approx 0.9 h^{-1}$ Mpc value advocated here. This is not surprising. Popesso et al. (2004) did not rely on red-sequence galaxy selection, which lowers the density contrast of galaxy clusters. Consequently, we expect the optimal aperture to move inwards. It is also worth noting that Popesso et al. (2004) report a scatter in L_X at fixed optical luminosity L_{opt} of $\sigma_{\ln L_X|L_{opt}} = 0.41$, which is much smaller than what we have achieved. We caution, however, that the Popesso et al. (2004) value has *not* been corrected for selection effects. Indeed, they also report $\sigma_{\ln L_{opt}|L_X} = 0.46$, with a scaling of $L_{opt} \propto L_X^\alpha$ with $\alpha = 0.45$. For power-law abundance functions, application of Bayes’s Theorem relates these two scatters via

$$\sigma_{\ln L_{opt}|L_X} = \alpha \sigma_{\ln L_X|L_{opt}}. \quad (28)$$

That this equality does not hold for Popesso et al. (2004) analysis is a direct consequence of having neglected selection effects. As a rough estimate, we expect for the scatter $\sigma_{\ln L_{opt}|L_X}$ to be more robust to X-ray selection — one finds all clusters of a given X-ray flux, but not all clusters of a given L_{opt} — so we can use equation 28 to estimate the corrected scatter in L_X at fixed L_{opt} . We find $\sigma_{\ln L_X|L_{opt}} = 0.46/0.45 = 1.02$. Given that Popesso et al. (2004) did not use color information when estimating optical luminosity, it is not surprising that the corrected scatter would be this large.

The scatter in X-ray luminosity at fixed richness for our final richness estimator is $\sigma_{\ln L_X|\lambda} = 0.63 \pm 0.02$. As was argued in Paper II, this scatter is likely dominated by the miscentering properties of the maxBCG cluster catalog, rather than by intrinsic scatter in the richness–mass relation. Consequently, we expect that making improvements to the centering algorithm used in cluster finding may result in a further reduction of the scatter in L_X at fixed richness.

We also performed extensive tests on the robustness of the richness estimator λ to the details of the measurement. We find that our richness estimator is robust to various modifications, including:

1. It is robust to the choice of optical bands used for color selection, provided the bands straddle the 4000 Å break.
2. It is robust to changes in the overall background normalization, for changes $\lesssim 50\%$ for the richest clusters.
3. It is robust to moderate changes in the intrinsic width of the red sequence.
4. It is robust to uncertainty in the photometric zero-point up to ± 0.1 mag.
5. It is robust to uncertainty in the color–redshift relation. In particular, consistent results can be obtained by fitting the red-sequence directly for each individual cluster as are obtained for the global model.

The uncertainty associated with most of these effects is $\Delta\lambda \approx 1 - 2$, which is significantly smaller than the intrinsic scatter of the richness–mass relation. Consequently, one can implement our optical richness estimator regardless of the details of the optical data at hand, and be confident that the resulting richness estimates can be fairly compared to those from other data sets. Appendix A contains a summary of how to implement our richness estimator λ . Finally, in order to try to improve its usefulness, we provide a preliminary mass–richness relation for λ in Appendix B. We emphasize that this mass calibration is preliminary, and that a robust calibration with well understood error must await for future work.

We believe that the method for calculating λ is close to an optimal richness estimator for photometric catalogs, while the parameters described here are optimized for this particular cluster sample. Importantly, this estimator can be applied irrespective of the cluster selection algorithm, while its robustness to the details of the implementation ensure that one can fairly compare different data sets. Moreover, the detailed understanding we have gained on how to properly estimate cluster richness and galaxy membership of galaxy clusters can help guide cluster finding efforts. Indeed, we are currently developing such a cluster finding algorithm. In short, we are confident that the detailed studies we have performed in this context will prove to be of critical importance for maximizing the cosmological utility of upcoming optical surveys such as the Dark Energy Survey, Pan-STARRS, and Hyper-SuprimeCam.

We thank Erica Ellingson for useful discussions and feedback, and Adam Mantz, Yu-Ying Zhang, and Graham Smith for help with the interpretation of their cluster masses and the corresponding systematic uncertainties. ESR thanks the TABASGO Foundation for support. This work was supported in part by the Director, Office of Science, Office of High Energy and Nuclear Physics, of the U.S. Department of Energy under Contract No. AC02-05CH11231. ER is funded by NASA through the Einstein Fellowship Program, grant PF9-00068. This material is based upon work supported by the National Science Foundation under Award No. AST-0902010. AEE acknowledges support from NSF AST-0708150 and NASA NNX07AN58G. RHW received support from the DOE under contract DE-AC03-76SF00515.

Funding for the SDSS and SDSS-II has been provided by the Alfred P. Sloan Foundation, the Participating Institutions, the National Science Foundation,

the US Department of Energy, the National Aeronautics and Space Administration, the Japanese Monbukagakusho, the Max Planck Society, and the Higher Education Funding Council for England. The SDSS Web site is <http://www.sdss.org/>

The SDSS is managed by the Astrophysical Research Consortium for the Participating Institutions. The Participating Institutions are the American Museum of Natural History, Astrophysical Institute Potsdam, University of Basel, University of Cambridge, Case Western Reserve University, University of Chicago, Drexel University, Fermilab, the Institute for Advanced Study, the

Japan Participation Group, Johns Hopkins University, the Joint Institute for Nuclear Astrophysics, the Kavli Institute for Particle Astrophysics and Cosmology, the Korean Scientist Group, the Chinese Academy of Sciences (LAMOST), Los Alamos National Laboratory, the Max-Planck-Institute for Astronomy (MPIA), the Max-Planck-Institute for Astrophysics (MPA), New Mexico State University, Ohio State University, University of Pittsburgh, University of Portsmouth, Princeton University, the United States Naval Observatory, and the University of Washington.

REFERENCES

- Abazajian, K. N. et al. 2009, *ApJS*, 182, 543
 Abraham, R. G. et al. 1996, *ApJ*, 471, 694
 Adelman-McCarthy, J. K. et al. 2006, *ApJS*, 162, 38
 Bartelmann, M. 1996, *A&A*, 313, 697
 Becker, M. R., & Kravtsov, A. V. 2010, *ArXiv e-prints*, 1011.1681
 Becker, M. R. et al. 2007, *ApJ*, 669, 905
 Berlind, A. A. et al. 2003, *ApJ*, 593, 1
 Bernardi, M., Sheth, R. K., Nichol, R. C., Schneider, D. P., & Brinkmann, J. 2005, *AJ*, 129, 61
 Böhringer, H. et al. 2004, *A&A*, 425, 367
 Bower, R. G., Lucey, J. R., & Ellis, R. S. 1992, *MNRAS*, 254, 601
 Boylan-Kolchin, M., Springel, V., White, S. D. M., & Jenkins, A. 2010, *MNRAS*, 406, 896
 Busha, M. T., Wechsler, R. H., Behroozi, P. S., Gerke, B. F., Klypin, A. A., & Primack, J. R. 2010, *ArXiv e-prints*, 1011.6373
 Chen, Y., Reiprich, T. H., Böhringer, H., Ikebe, Y., & Zhang, Y.-Y. 2007, *A&A*, 466, 805
 De Lucia, G. et al. 2007, *MNRAS*, 374, 809
 Dressler, A. 1984, *ARA&A*, 22, 185
 Ebeling, H., Edge, A. C., Allen, S. W., Crawford, C. S., Fabian, A. C., & Huchra, J. P. 2000, *MNRAS*, 318, 333
 Ebeling, H., Edge, A. C., Böhringer, H., Allen, S. W., Crawford, C. S., Fabian, A. C., Voges, W., & Huchra, J. P. 1998, *MNRAS*, 301, 881
 Eisenhardt, P. R. M. et al. 2008, *ApJ*, 684, 905
 Eisenstein, D. J. et al. 2001, *AJ*, 122, 2267
 Gladders, M. D., & Yee, H. K. C. 2000, *AJ*, 120, 2148
 Hansen, S. M., McKay, T. A., Wechsler, R. H., Annis, J., Sheldon, E. S., & Kimball, A. 2005, *ApJ*, 633, 122
 Hansen, S. M., Sheldon, E. S., Wechsler, R. H., & Koester, B. P. 2009, *ApJ*, 699, 1333
 Hao, J. et al. 2009, *ApJ*, 702, 745
 Hockney, R. W., & Eastwood, J. W. 1981, *Computer Simulation Using Particles* (Computer Simulation Using Particles, New York: McGraw-Hill, 1981)
 Hogg, D. W. et al. 2004, *ApJ*, 601, L29
 Hu, W., & Kravtsov, A. V. 2003, *ApJ*, 584, 702
 Johnston, D. E. et al. 2007, *ArXiv e-prints*, 709, astro-ph/0709.1159
 Kaiser, N. 1986, *MNRAS*, 222, 323
 Kelly, B. C. 2007, *ApJ*, 665, 1489
 Kodama, T., & Arimoto, N. 1997, *A&A*, 320, 41
 Koester, B. P. et al. 2007a, *ApJ*, 660, 239
 —. 2007b, *ApJ*, 660, 221
 Kormendy, J., & Djorgovski, S. 1989, *ARA&A*, 27, 235
 Kravtsov, A. V., Berlind, A. A., Wechsler, R. H., Klypin, A. A., Gottlöber, S., Allgood, B., & Primack, J. R. 2004, *ApJ*, 609, 35
 Lima, M., & Hu, W. 2005, *Phys. Rev. D*, 72, 043006
 Lin, Y.-T., & Mohr, J. J. 2004, *ApJ*, 617, 879
 Lopes, P. A. A., de Carvalho, R. R., Capelato, H. V., Gal, R. R., Djorgovski, S. G., Brunner, R. J., Odewahn, S. C., & Mahabal, A. A. 2006, *ApJ*, 648, 209
 Mantz, A., Allen, S. W., Ebeling, H., Rapetti, D., & Drlica-Wagner, A. 2010, *MNRAS*, 406, 1773
 Maughan, B. J. 2007, *ApJ*, 668, 772
 Mortonson, M. J., Hu, W., & Huterer, D. 2011, *Phys. Rev. D*, 83, 023015
 Navarro, J. F., Frenk, C. S., & White, S. D. M. 1995, *MNRAS*, 275, 56
 Oguri, M., & Takada, M. 2011, *Phys. Rev. D*, 83, 023008
 O’Hara, T. B., Mohr, J. J., Bialek, J. J., & Evrard, A. E. 2006, *ApJ*, 639, 64
 Popesso, P., Biviano, A., Böhringer, H., & Romaniello, M. 2007, *A&A*, 464, 451
 Popesso, P., Biviano, A., Böhringer, H., Romaniello, M., & Voges, W. 2005, *A&A*, 433, 431
 Popesso, P., Böhringer, H., Brinkmann, J., Voges, W., & York, D. G. 2004, *A&A*, 423, 449
 Postman, M., Lubin, L. M., Gunn, J. E., Oke, J. B., Hoessel, J. G., Schneider, D. P., & Christensen, J. A. 1996, *AJ*, 111, 615
 Reyes, R., Mandelbaum, R., Hirata, C., Bahcall, N., & Seljak, U. 2008, *MNRAS*, 390, 1157
 Rozo, E. et al. 2009a, *ApJ*, 699, 768
 —. 2009b, *ApJ*, 703, 601
 Rozo, E., Rykoff, E. S., Koester, B. P., Nord, B., Wu, H., Evrard, A. E., & Wechsler, R. H. 2011, *arXiv*, xXXXX
 Rozo, E. et al. 2007, *ArXiv Astrophysics e-prints*, astro-ph/0703571
 —. 2010a, *ApJ*, 708, 645
 Rozo, E., Wu, H., & Schmidt, F. 2010b, *ArXiv e-prints*, 1009.0756
 Rykoff, E. S. et al. 2008, *ApJ*, 675, 1106
 Scranton, R. et al. 2002, *ApJ*, 579, 48
 Shaw, L. D., Holder, G. P., & Dudley, J. 2010, *ApJ*, 716, 281
 Sheldon, E. S. et al. 2009a, *ApJ*, 703, 2217
 —. 2009b, *ApJ*, 703, 2217
 Strauss, M. A. et al. 2002, *AJ*, 124, 1810
 Takada, M. 2010, in *American Institute of Physics Conference Series*, Vol. 1279, American Institute of Physics Conference Series, ed. N. Kawai & S. Nagataki, 120–127
 Tinker, J., Kravtsov, A. V., Klypin, A., Abazajian, K., Warren, M., Yepes, G., Gottlöber, S., & Holz, D. E. 2008, *ApJ*, 688, 709
 Vikhlinin, A. et al. 2009, *ApJ*, 692, 1033
 Voges, W. et al. 1999, *A&A*, 349, 389
 Wetzell, A. R., & White, M. 2010, *MNRAS*, 403, 1072
 York, D. G. et al. 2000, *AJ*, 120, 1579
 Zhang, Y., Finoguenov, A., Böhringer, H., Kneib, J., Smith, G. P., Kneissl, R., Okabe, N., & Dahle, H. 2008, *A&A*, 482, 451
 Zhang, Y. et al. 2010, *ApJ*, 711, 1033
 Zheng, Z. et al. 2005, *ApJ*, 633, 791

APPENDIX

A USER FRIENDLY GUIDE FOR IMPLEMENTING THE RICHNESS ESTIMATOR λ

In this appendix, we lay out the “recipe” for implementing the richness estimator λ . First, we list the “ingredients” that are necessary, followed by the “cooking instructions.” As described in Section 5, several substitutions for certain ingredients can be made without a significant effect on the richness parameter. We make note of the possible

substitutions below.

Ingredients

1. All galaxies within $\sim 1.25 h^{-1}$ Mpc of the cluster center. The richest maxBCG cluster has $\lambda = 216$ and $R_c = 1.17 h^{-1}$ Mpc, so this is the largest size that is needed.
2. If the cluster redshift z is between 0.1 and 0.3, you will need the $g - r$ color (c) of each galaxy. As described in Section 5.1, any pair of sensitive bands that straddle the 4000 Å break may be substituted. Similarly, if you work at higher or lower redshift, you will need to change your filter appropriately.
3. The i -band magnitude of each galaxy, or a suitable red filter.
4. The k -corrected value of $0.2L_*$ for the band in question. For SDSS i -band and $0.05 < z < 0.35$, $m_*(z)$ is well described by Eqn. 11, and the luminosity cut is given as $m_* + 1.75$ mag.
5. The mean galaxy background as a function of color and magnitude (see Sections 3.4 and 5.2).
6. The ridgeline slope and intercept, as described in Eqn. 23. Alternatively, you can fit for the ridgeline slope and intercept with $\sigma_{\text{int}} = 0.05$ from the list of galaxies.

“Baking” Instructions

1. Calculate the luminosity filter value for each galaxy, $\phi(m)$, as described in Eqn. 10 in Section 3.2. Note that the filter is normalized such that the integral from $m = -\infty$ to m_{cut} is exactly one.
2. Calculate the radial filter value for each galaxy, $2\pi R\Sigma(R)$, as described in Eqn. 6 in Section 3.1. The radial filter needs to be normalized by integrating R_c as per equation 8. Thus, the amplitude of $\Sigma(R)$ is a function of R_c , with the normalization constant for the particular implementation of the NFW profile adapted in this work given in Eqn. 9.
3. Calculate the color filter value for each galaxy, $G(c, m|z)$, as described in Eqn. 21 in Section 4.3.
4. Calculate the background filter value for each galaxy, $b(m, c) = 2\pi R\bar{\Sigma}_g(m, c)/C(z)^2$. We have defined $\bar{\Sigma}_g(m, c)$ as the mean galaxy background in $N/\text{sq.deg./mag/mag}$, and the conversion factor $C(z)$ is given in degrees/Mpc at the redshift of the cluster.
5. Using a zero-finder (e.g., bisector or Newton’s method), solve the following equation:

$$0 = \lambda - \sum_{R < R_c(\lambda)} p_i \quad (\text{A1})$$

where

$$p_i = \frac{\lambda 2\pi R_i \Sigma(R_i) \phi(m_i) G(c_i)}{\lambda 2\pi R_i \Sigma(R_i) \phi(m_i) G(c_i) + b(m_i, c_i)} \quad (\text{A2})$$

and

$$R_c(\lambda) = R_0(\lambda/100.0)^\beta. \quad (\text{A3})$$

Note that once the root λ of equation A1 has been found, equation A2 can be used to estimate the membership probability of every galaxy.

6. To estimate the statistical error in λ , use equation 3. This measurement error is typically very small, of order $\Delta\lambda/\lambda = 0.4\lambda^{-1/2}$, or $\approx 4\%$ (9%) for $\lambda = 100$ (15).

Sample IDL code that will calculate λ for SDSS data is available at <http://kipac.stanford.edu/maxbcg/>

THE MASS–RICHNESS RELATION

The goal of this paper was to extensively test and optimize the richness measure proposed by Rozo et al. (2009b). A careful calibration of the mass–richness relation is beyond the scope of the current paper, though we do intend to address this problem in subsequent work. Nevertheless, we felt it was important to provide a rough calibration that may be used for comparison purposes, and to test the efficacy of our estimator. To this end, we have relied on abundance matching techniques. Briefly, we compute the cumulative cluster abundance function $N_{\text{clusters}}(> \lambda)$, defined as the number of maxBCG clusters of richness λ or higher. We then also compute the expected cumulative mass function $N_{\text{halos}}(> m)$ as a function of mass by integrating the Tinker et al. (2008) mass function for our fiducial cosmology over the maxBCG survey volume.²² When computing the mass function, we adopt as our fiducial mass definition M_{200m} , the mass contained within a 200 overdensity relative to the mean matter density. A cluster of richness

²² maxBCG clusters probe the redshift region $z \in [0.1, 0.3]$ over a survey area $\Omega = 2.25356$ sr.

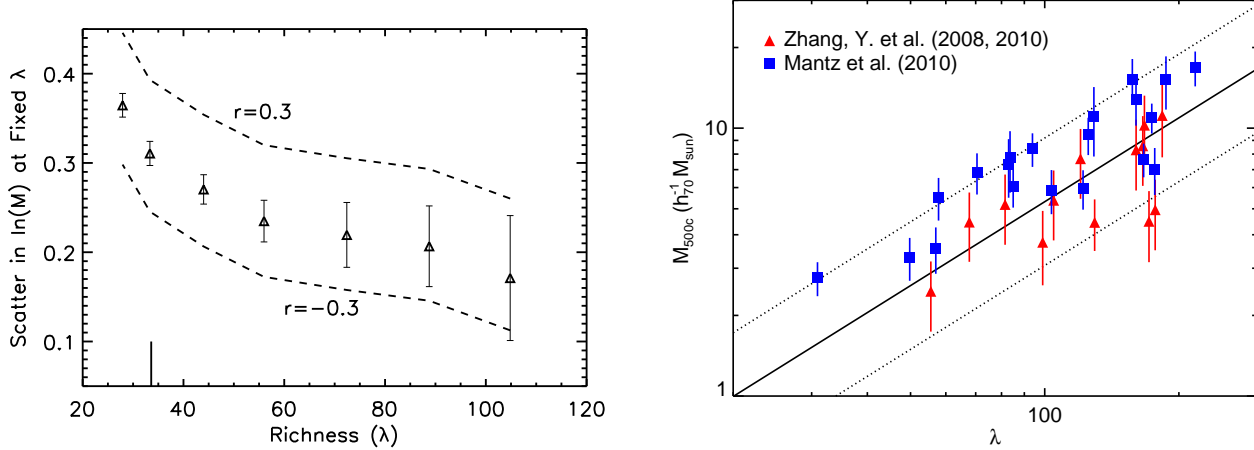


FIG. B10.— *Left*: The scatter in mass at fixed richness, as estimated via equation B2. The scatter is estimated using all clusters above a given richness, as opposed to using narrowly binned samples. The triangles with error bars show the recovered scatter assuming $r = 0$, while the dashed lines illustrate how the scatter changes as we vary the correlation coefficient between L_X and λ at fixed mass. The small vertical solid line along the x axis marks the richness threshold for the top-2000 clusters. Below this richness, we expect the scatter is compromised due to the original maxBCG selection. *Right*: Mass as a function of λ obtained via density matching, scaled to M_{500c} (Eqn. B6). Dotted lines are the expected 90% scatter contours obtained from the X-ray constraints. For reference, X-ray masses from two cluster samples that overlap the maxBCG footprint are overplotted. Blue squares are from BCS sample (Mantz et al. 2010), and red triangles are from the LoCuSS sample (Zhang et al. 2008, 2010). See text for discussion of the possible origin of the normalization offsets between the two data sets. In each case, the observed mass scatter agrees well with the predicted mass scatter.

λ is assigned a mass M by solving the equation $N_{\text{clusters}}(> \lambda) = N_{\text{halos}}(> M)$ for $M(\lambda)$. We call this mass estimate the *density matching* mass, denoted $M_{\text{dm}}(\lambda)$.

As detailed in Mortonson et al. (2011), mass estimates from density matching are expected to be biased *high* relative to the Bayesian posterior by an amount equal to $\frac{1}{2}\gamma\sigma^2$ in the log. Here, γ is the slope of the halo mass function at mass M , and σ is the scatter in mass at fixed richness. Thus, in order to correct for this bias, we must first estimate the scatter in mass at fixed richness for λ . To do so, we rely on the scatter in L_X at fixed richness. Assuming $\ln L_X = a + \alpha \ln M$, it follows that a scatter in mass $\sigma_{M|\lambda}$ corresponds to a scatter in L_X given by $\alpha\sigma_{M|\lambda}$. If L_X and λ are uncorrelated, then on simply needs to add in quadrature the intrinsic scatter in L_X at fixed mass, $\sigma_{L_X|M}$, to arrive at the total scatter in L_X at fixed richness:

$$\sigma_{L_X|\lambda}^2 = \sigma_{L_X|M}^2 + \alpha_{L_X|M}^2 \sigma_{M|\lambda}^2. \quad (\text{B1})$$

With this equation, one can straightforwardly solve for $\sigma_{M|\lambda}$. In the slightly more general case when L_X and λ are correlated, one finds

$$\sigma_{M|\lambda} = r\sigma_{M|L_X} + \left[\frac{\sigma_{L_X|\lambda}^2}{\alpha_{L_X|M}^2} - \sigma_{M|L_X}^2(1 - r^2) \right]^{1/2}. \quad (\text{B2})$$

In the above equation, r is the unknown correlation coefficient between the richness λ and L_X at fixed mass, while $\alpha_{L_X|M}$ is the slope of the $L_X - M$ relation. We adopt the fiducial values $\alpha_{L_X|M} = 1.61$ and $\sigma_{M|L_X} = 0.246$ as per Vikhlinin et al. (2009). As for the correlation coefficient r , because the scatter in L_X is dominated by emission from the core, we do not expect λ and L_X to be strongly correlated. Here, we simply consider three values for r , $r = \pm 0.3$, and $r = 0$. Setting the scatter $\sigma_{L_X|\lambda} = 0.63$ as appropriate for our top 2000 clusters, we arrive at $\sigma_{M|\lambda} = 0.31^{+0.08}_{-0.07}$, where the error bars reflect the change in the scatter for $r = \pm 0.3$. Figure B10 (left panel) illustrates how our recovered scatter $\sigma_{M|\lambda}$ changes as a function of the minimum richness λ of the sample under consideration.

One interesting feature of the scatter in mass at fixed richness as a function of λ is that the scatter appears to increase slowly with decreasing richness for $\lambda \gtrsim 60$, but begins to climb much faster below $\lambda \lesssim 60$. Remarkably, in Paper II we found that $\lambda \approx 60$ is the richness at which the miscentering of maxBCG galaxy clusters is expected to become important. Moreover, as we argue in Paper II, cluster miscentering “turns-on” very quickly. Consequently, it is possible that the rapid rise of the scatter with decreasing richness below $\lambda \lesssim 60$ does not reflect the true intrinsic scatter of the estimator λ , but is rather a reflection of the miscentering properties of maxBCG clusters. Above $\lambda \gtrsim 60$, however, we do not expect cluster miscentering to play as significant a role. Thus, it is likely that the observed scatter at $\lambda \gtrsim 60$ is close to the intrinsic scatter of our richness estimator.

Based on the results shown in Figure B10 (left panel), we adopt a fiducial scatter $\sigma_{M|\lambda} = 0.25$. With this scatter in hand, we can correct the density matched masses by the expected bias. If $M_{\text{dm}}(\lambda)$ is the density matched mass of a cluster of richness λ , we set the cluster’s final mass to

$$M(\lambda) = \exp\left(-\frac{1}{2}\gamma(M_{\text{dm}}(\lambda))\sigma_{M|\lambda}^2\right) M_{\text{dm}}(\lambda) \quad (\text{B3})$$

where $\gamma(M_{\text{dm}})$ is the slope of the halo mass function $dN/d\ln M \propto M^{-\gamma}$ evaluated at the density matching mass M_{dm} . Having assigned a mass to every cluster in this fashion, the resulting mass–richness relation is fit to a power-law using all clusters of richness $\lambda \geq 60$. We restrict ourselves to these clusters given that we believe cluster miscentering might be starting to become important below this richness. We finally arrive at

$$\ln\left(\frac{M_{200m}}{h_{70}^{-1} 10^{14} M_{\odot}}\right) = 1.72 + 1.08 \ln(\lambda/60). \quad (\text{B4})$$

Note that we have scaled the masses relative to $h = H_0/100 \text{ km s}^{-1} \text{ Mpc}^{-1} = 0.7$, and we have made explicit that this scaling relation is appropriate for a mass overdensity of 200 relative to the mean matter density. Equation B4 is our proposed scaling between mass and richness, while $\sigma_{M|\lambda} = 0.25$ is our fiducial value for the scatter in mass at fixed richness. This value may be somewhat overestimated at the high mass end. Note, however, that the amplitude A of this relation can shift by ≈ 0.1 depending on the value of the correlation coefficient r , the choice of fiducial cosmology, etc. Adopting a 20% systematic uncertainty the overall amplitude, and adding in quadrature to the expected statistical uncertainty $\sigma_{M|\lambda} = 0.25$, we find that the total uncertainty in the mass of any given cluster is ≈ 0.33 at the 1σ level.

We can also compute the corresponding mass–richness relations for other mass definitions by rescaling all assigned cluster masses using the formulas in Hu & Kravtsov (2003), and refitting to a power-law. We find

$$\ln\left(\frac{M_{200c}}{h_{70}^{-1} 10^{14} M_{\odot}}\right) = 1.48 + 1.06 \ln(\lambda/60) \quad (\text{B5})$$

$$\ln\left(\frac{M_{500c}}{h_{70}^{-1} 10^{14} M_{\odot}}\right) = 1.14 + 1.04 \ln(\lambda/60). \quad (\text{B6})$$

We emphasize again, however, that these are *not* meant to be a rigorous mass calibration, a problem that we defer to future work.

As a check of our mass calibration, we have assembled two cluster samples that overlap the maxBCG footprint and redshift range. The first sample is drawn from the LoCuSS observations of high luminosity clusters from RASS cluster catalogs (Ebeling et al. 1998, 2000; Böhringer et al. 2004). These clusters have been observed with both *XMM/Newton* to obtain hydrostatic mass estimates (Zhang et al. 2008, 2010), with *Subaru* weak lensing follow-up to provide independent estimates of the masses of several clusters (Zhang et al. 2010). Here we concentrate on the hydrostatic mass estimates of Zhang et al. (2008, 2010). The *ROSAT* Brightest Cluster Sample (BCS; Ebeling et al. 1998) has been observed with *Chandra*, with hydrostatic mass estimates obtained by Mantz et al. (2010). The X-ray mass values for the BCS clusters have been reduced by 11% to account for the *Chandra* calibration update described in that paper (Mantz, A., private comm.). For each cluster, we have used the X-ray center and spectroscopic redshift to estimate λ from SDSS DR7 photometric data. We emphasize that we cannot use this data to provide a rigorous mass calibration due to the fact that these cluster samples do not constitute a random sampling of the maxBCG clusters. We only use this data for illustrative purposes, and to test whether the mass calibration derived from density matching is reasonable.

Figure B10 (right panel) shows the mass as a function of λ obtained via density matching, scaled to M_{500c} (Eqn. B6). Dotted lines are the expected 90% confidence interval assuming an uncertainty $\Delta \ln M = 0.33$ as discussed above (25% intrinsic scatter, 20% systematic uncertainty). The LoCuSS sample is overplotted with red triangles, and the BCS clusters are shown with blue squares. It is clear that there is a normalization offset between the two data sets, which corresponds to a systematic offset $\Delta \ln M = 0.45$ in mass. A full accounting of this offset is beyond the scope of this paper, but there are several possibilities. First, the analyses were done with different data sets (*XMM* and *Chandra*); second, there is an additional 10% systematic uncertainty in the normalization of the BCS clusters due to the uncertainty in f_{gas} used to calculate the masses; third, because the masses are calculated in a scaled aperture (r_{500c}), any slight normalization offset is magnified in the full analysis; fourth, Zhang et al. (2008) note that if one changes their parametrization of the temperature profile below $\approx 0.5 R_{500}$ so as to allow for a rapid drop in the cluster temperature, their hydrostatic masses can increase by as much as 25%.

Regardless of what the ultimate source of the difference in the normalization between the two data sets is, it is reassuring to see that our rough mass calibration fits between these two data sets. Moreover, the scatter in the mass–richness relation is clearly smaller than the overall difference in normalization between the two sets, and consistent with our 25% estimate for the scatter. This demonstrates both that the richness estimator λ is indeed tightly correlated with cluster mass with scatter at the $\sim 20\% - 30\%$ level, and that our 33% estimate for the uncertainty in the mass of any one cluster is reasonable. Note that since the scatter in mass at fixed richness for the original maxBCG richness (N_{200}) was estimated to be $\sigma_{\ln M|N} = 0.45$ Rozo et al. (2009a), this means that even this rough mass calibration allows us to predict individual cluster masses with significantly higher precision than we could using the maxBCG richness.

THE AUGMENTED MAXBCG CLUSTER CATALOG

Table C2 contains the improved richness, λ , for each cluster in the maxBCG cluster catalog. The positions (RA, Dec), photometric redshifts (z), and original richness estimate (N_{200}) are taken directly from Table 1 in Koester et al. (2007a). The spectroscopic redshifts ($z_{\text{spec}}^{\text{BCG}}$), are obtained by cross-identifying the maxBCG BCG positions with the full spectroscopic catalog from SDSS DR8²³, thus increasing the number of BCGs with spectra from 5413 to 9409.

²³ <http://www.sdss.org/dr8/spectro/>

TABLE C2. MAXBCG CLUSTER CATALOG WITH λ RICHNESS

R.A. (deg)	Decl. (deg)	z	$z_{\text{spec}}^{\text{BCG}}$	N_{200}	λ	λ_e
239.58334	27.233419	0.103	0.091	188	199.82	3.84
140.10742	30.494063	0.292	-1.000	126	181.24	6.22
198.77182	51.817380	0.286	-1.000	87	172.22	5.00
126.37104	47.133478	0.135	0.129	99	147.35	3.72
203.16008	50.559919	0.284	-1.000	114	174.03	5.71
354.41554	0.271383	0.286	0.277	88	129.53	4.85
213.78496	-0.493247	0.135	0.139	115	77.89	3.34
189.24684	63.186584	0.294	-1.000	89	114.17	4.81
216.48612	37.816455	0.167	0.170	98	118.92	3.62
187.70363	10.546381	0.167	0.170	70	120.36	4.07

NOTE. — A full electronic version of Table C2 in fits format is available at <http://kipac.stanford.edu/maxbcg/>. A portion is shown here for guidance regarding its form and content.

Finally, the improved richness and error estimates (λ , λ_e) are taken from this work. Note that the catalog is complete in N_{200} , but is not complete in λ . We set $z_{\text{spec}}^{\text{BCG}} = -1.0$ when a spectrum is not available, and set $\lambda = -1.0$ when no significant number of red galaxies above background is found by the richness estimator. In addition, we note that the DR7 galaxy catalog used to calculate λ covers a slightly different footprint than the original DR4 catalog used to construct the original maxBCG catalog. There are 80 maxBCG clusters that we cannot calculate reliable richness estimates as they are in newly masked regions. For these, we set $\lambda = -2.0$ in the catalog.